Experimental Eye Research 272 (2026) 111177

Contents lists available at ScienceDirect

Experimental Eye Research

journal homepage: www.elsevier.com/locate/yexer

Research article

Sirtuin 1 induced VEGF-A overexpression along with increased pericyte coverage and basement membrane alterations in mouse retina

Joana Catita [a,b], Andreia Valença [a,b,c,d,e], Mariana López-Luppo [a,f], Víctor Nacher [a,f], Aina Bonet [a,g], Ana Carretero [a,f], Patricia Jaramillo-Garcés [a,f], Marc Navarro [a,f], Fernando Faus [h], Luísa Mendes-Jorge [a,c,d], David Ramos [a,c,i,*], Jesús Ruberte [a,f,**]

[a] Center for Animal Biotechnology and Gene Therapy, Universitat Autònoma de Barcelona, Bellaterra, Spain
[b] Research in Veterinary Medicine (I-MVET), Faculty of Veterinary Medicine, Lusófona University - Lisbon University Centre, Lisbon, Portugal
[c] CIISA - Centre for Interdisciplinary Research in Animal Health, Faculty of Veterinary Medicine, Universidade de Lisboa, Lisbon, Portugal
[d] Laboratório Associado para Ciência Animal e Veterinária (AL4AnimalS), Portugal
[e] Superior School of Health, Protection and Animal Welfare, Polytechnic Institute of Lusophony, Lisbon, Portugal
[f] Department of Animal Health and Anatomy, Faculty of Veterinary, Universitat Autònoma de Barcelona, Bellaterra, Spain
[g] Institute for Research in Biomedicine (IRB Barcelona), The Barcelona Institute of Science and Technology (BIST), Barcelona, Spain
[h] Department of Ophthalmology, Hospital Universitario Miguel Servet, Zaragoza, Spain
[i] Department of Morphological Sciences, School of Medicine, Universitat Autònoma de Barcelona, Bellaterra, Spain

ARTICLE INFO

Keywords:
Sirtuin 1
VEGF
Pericyte
Basement membrane
Vessel stabilization

ABSTRACT

Sirtuin 1 is of main importance in vascular homeostasis maintenance and in the protection of microcirculatory function during pathology. However, the exact mechanisms underlying the protective effects of Sirtuin 1 on retinal vasculature are still not fully understood. Here, we analyse the effects of Sirtuin 1 overexpression in the retina of transgenic mice. Mice retinas were studied by means of PCR, Western blot and immunohistochemistry to assess the expression of Sirtuin 1, VEGF-A, and the PDGF-B/PDGFR-β pathway. Retinal vasculature was deeply analysed by immunohistochemistry, trypsin digestion, and transmission electron microscopy. Our results showed that Sirtuin 1-tg mice exhibited a moderate retinal Sirtuin 1 overexpression throughout the retinal parenchyma, mainly at the nuclei of vascular retinal cells. This Sirtuin 1 overexpression led to an increased expression of retinal VEGF-A. In addition, our results suggested that the expected VEGF-driven angiogenesis was prevented in Sirtuin 1-tg mice retinas by two vessel stabilization mechanisms: increased pericyte coverage, and focal increased collagen IV deposition in blood vessel basement membrane. Altogether, our findings may indicate a possible role for Sirtuin 1 in modulating VEGF angiogenic effects, potentially being associated with changes in pericyte coverage and basement membrane protein deposition in retinal blood vessels.

1. Introduction

Pericytes are branched cells residing in the capillary wall, where they are integrated within the basement membrane and wrap endothelial cells, with which they establish strong physical contact (Zimmerman, 1923; Armulik et al., 2011; Caporarello et al., 2019). Despite this common definition, pericytes constitute a heterogeneous population with different origins, morphology, and function among organs and even within the vasculature of one organ. In this regard, several morphologically distinct types of pericytes have been described, such as, ensheathing pericytes, mesh pericytes and thin strand pericytes in the central nervous system (Grant et al., 2019; Hartmann et al., 2022). Moreover, the ratio of pericytes to endothelial cells also varies through the body, being maximal (1:1) at the retina where they play a crucial role in the composition of blood retinal barrier (Shepro and Morel, 1993). Pericytes are essential for the process of vessel stabilization (Gerhard and Betsholtz, 2003), which is defined as the envelopment of pericytes around the endothelial cells and formation of extracellular

* Corresponding author. Department of Morphological Sciences, School of Medicine Universitat Autònoma de Barcelona Avda. de Can Domènech Bellaterra, Barcelona, 08193, Spain.
** Corresponding author. Center for Animal Biotechnology and Gene Therapy Universitat Autònoma de Barcelona C/ de la Vall Moronta Bellaterra, Barcelona, 08193, Spain.
E-mail addresses: David.ramosgonzalez@uab.cat (D. Ramos), jesus.ruberte@uab.cat (J. Ruberte).

https://doi.org/10.1016/j.exer.2026.111177
Received 11 May 2026; Received in revised form 9 June 2026; Accepted 19 July 2026
Available online 31 July 2026
0014-4835/© 2026 The Authors. Published by Elsevier Ltd. This is an open access article under the CC BY-NC-ND license (http://creativecommons.org/licenses/by-nc-nd/4.0/).

matrix, including the basement membrane (Hirschi et al., 1997; Diaz-Flores et al., 2009). During angiogenesis, pericytes are recruited following growth factor signalling, such as PDGF-B released from angiogenic endothelial cells that binds to PDGFR-β located on pericytes surface (Hellström et al., 1999; Betsholtz, 2004). It is accepted that pericyte loss is the earliest cellular event and a hallmark of diabetic retinopathy (Armulik et al., 2005). Pericyte disappearance during diabetes is associated with the disruption in the crosstalk between pericytes and endothelial cells (Li et al., 2025). Interestingly, chronic hyperglycemia during diabetes causes decreases in the expression of PDGF-B (Tanii et al., 2006; Kolluru et al., 2012; Mercier et al., 2021). According to these data, preventing the loss of pericytes may help mitigate the course of diabetic retinopathy.

Sirtuin 1 (Sirt1) is a class III histone deacetylase that interacts with target proteins and regulates many cellular functions including cell metabolism, stress response, cell cycle, senescence, and cell death pathways (Brooks and Gu, 2009; Hwang et al., 2013; Li et al., 2014; Chang and Guarente, 2014). Sirt1 resides primarily in the cell nucleus (Michishita et al., 2005; Michan and Sinclair, 2007), but it may also be found in the cytoplasm (Finkel et al., 2009). Sirt1 has broad physiological functions in proliferation, metabolism, and aging (Law et al., 2024). In microcirculation, Sirt1 plays an important role in maintaining vascular homeostasis and protecting microcirculatory function under pathological conditions (Law et al., 2024). In this regard, Sirt1 prevents vascular senescence (Orimo et al., 2009), suppresses vascular inflammation (Stein et al., 2010; Oellerich and Potente, 2012), and controls postnatal angiogenic response and vascular growth (Potente et al., 2007; Oellerich and Potente, 2012). Although the proangiogenic effect has been demonstrated in many studies, it has also been evidenced that Sirt1 suppresses pathological angiogenesis (Law et al., 2024). In the retina, Sirt1 is expressed by neurons (Jaliffa et al., 2009) and is known for its protective effect against retinal diseases (Chen et al., 2013; D'Onofrio et al., 2015). Sirt1 expression and activity are decreased in human capillaries during diabetic retinopathy (Kowluru et al., 2014), and neuronal Sirt1 mediates retinal vascular regeneration in oxygen induced ischemic retinopathy (Chen et al., 2013). Nevertheless, despite all these clues, the exact mechanisms underlying the protective effects of Sirt1 on retinal vasculature are still not fully understood.

The objective of this study is to examine the potential involvement of Sirt1 in VEGF overexpression in retinal blood vessels. Our findings suggest that the expected VEGF-driven angiogenesis may be modulated by increased pericyte coverage and focal deposition of collagen IV in the capillary basement membrane, which contribute to vessel stabilization and a reduction in angiogenic activity.

2. Materials and methods

2.1. Mice

Fourth-to eight-month-old Sirt1 transgenic (Sirt1-tg) mice yielded from M. Serrano (Alto Labs, Cambridge, UK) and wild type (WT) littermates were used. As previously described (Pfluger et al., 2008), the upregulation of murine Sirt1 gene was directed by its endogenous promoter regions cloned into the BAC (Bacterial Artificial Chromosome) vector pBAC3.6. In this study, we used Sirt1 heterozygous mice, obtained by backcrossing Sirt1-tg mice with C57BL/6 J mice to preserve a common genetic background in all mice. All offspring were genotyped by performing PCR analysis using GoTaq® G2 Flexi DNA Polymerase Kit (Promega, Madison, WI, USA) from genomic DNA from mouse tails with specific oligonucleotide primers sequences detailed in Table 1. Mice had *ad libitum* access to water and a standard diet (2018S TEKLAD Global, Harlan Teklad, Madison, WI, USA). Controlled 12-h light/dark cycles and temperature conditions were ensured. Isoflurane overdose was used as the method of euthanasia (Fluothane®, AstraZeneca Farmacéutica Spain S.A., Madrid). ARVO Statement for the Use of Animals in Ophthalmic and Vision Research and the ARRIVE (Animal Research: Reporting In Vivo Experiments) guidelines 2.0 were followed for animal care and experimental procedures. All procedures were approved by the Ethics Committee in Animal and Human Experimentation of the Universitat Autònoma de Barcelona (FUE-2018-00717,286).

Table 1
Primers sequences for genotyping mouse tail DNA. F: forward; R: reverse.

Mice	Target	Direction	Sequence (5′ to 3′)	Reference
Sirt1-tg	p-BAC	F	AGATAGTTCACCGGGGTGAGAA	Pfluger et al. (2008)[29]
		R	TTCGGTCGAAGAGTATCTGGTG	
	Internal Positive Control	F	CTACATGAGCAGGCAGACTGGA	
		R	AATGGACGGGCTGCTTCTATC	
		R	CGTCCCTTGTAATGTTTCCC	

2.2. Gene expression analysis by quantitative real-time PCR (q-RT-PCR)

Gene expression was analysed by quantitative real-time polymerase chain reaction (q-RT-PCR) as previously reported (Valença et al., 2021). Briefly, RNA was extracted from freshly dissected retinas in a RNAse-free environment and reverse transcribed into cDNA. Corresponding PCRs were performed using a T100 or CFX384 Thermal cycler (Bio-Rad). Oligonucleotide primers sequences (PrimePCR SYBR Green Assay, Bio-Rad) used are listed in Table 2. Measurements were made in triplicate and relative expression was compared by statistical analysis.

2.3. Western blot analysis

Western blot analyses were performed in a homogenized pool of 6 retinas dissected from 6 different animals per group (Sirt1-tg and wild type). Procedures were as previously reported (Valença et al., 2021). Primary antibodies and dilutions used in this study were: rabbit anti-mouse Sirt1 (1:200; Abcam, Cambridge, UK); goat anti-mouse vascular endothelial growth factor-A (VEGF-A) (1:100, Santa Cruz Biotechnology, Santa Cruz, CA, USA); rabbit anti-mouse platelet-derived growth factor-B (PDGF-B) (1:500; Abcam); rabbit anti-mouse platelet-derived growth factor receptor-β (PDGFR-β) (1:1000; Abcam); rabbit anti-mouse collagen IV (1:500; Merck Millipore); and rabbit anti-mouse α-tubulin (1:500,000; Abcam). Horseradish peroxidase (HRP)-conjugated goat anti-rabbit IgG (Bionova Scientific, Fremont, CA, USA) at 1 : 5000 dilution, or HRP-conjugated rabbit anti-goat IgG (Dako, Glostrup, Denmark) at 1 : 10,000 dilution secondary antibodies were used as secondary antibodies. Values for densitometry analysis corresponded to the means of relative expression (normalized to WT) from 3 repetitions of Western blot experiments.

2.4. Immunohistochemistry

Paraffin embedded sections (3 μm) of mouse eyes were deparaffinized and rehydrated. Mouse retinal whole mounts were fixed in 10% neutral buffered formalin (NBF) for 2 h at 4°C. Paraffin sections and whole mount retinas were incubated overnight at 4°C with the following antibodies and dilutions: rabbit anti-mouse Sirt1 (1:50; Santa Cruz Biotechnology); goat anti-mouse collagen IV (1:20; Sta. Cruz); rabbit

Table 2
Primers sequences for qRT-PCR. F: forward; R: reverse.

Target	Direction	Sequence (5′ to 3′)	Reference
36B4	F	GGCCCTGCACTCTCGCTTT	García et al., 2009[81]
	R	TGCCAGGACGCGCTTGT	
SIRT1	F	GATGACAGAACGTCACACGC	Sapcariu, 2016[82]
	R	ATTGTTCGAGGATCGGTGCC	
VEGF-A$_{164}$	F	AGACAGAACAAAGCCAGAAAATCAC	Elias, Franckhause and Bosch, 2013[83]
	R	CACGTCTGCGGATCTTGGAC	
VEGF-A	F	ACTGGACCCTGGCTTTACTG	Albrecht et al., 2010[84]
	R	TCTGCTCTCCTTCTGTCGTG	

anti-mouse collagen IV (1:100; Merck Millipore); rat anti-mouse CD34 (1:50; Biolegend, San Diego, CA, USA); goat anti-mouse α smooth muscle actin (αSMA) (1:100; Abcam); rabbit anti-mouse neuron glial antigen-2 (NG2) (1:100; Merck Millipore); goat anti-mouse VEGF-A (1:50; Santa Cruz Biotechnology); rabbit anti-mouse PDGFR-β (1:100; Abcam); goat anti-mouse brain-specific homeobox/POU domain protein 3a (Brn3a) (1.50; Santa Cruz Biotechnology); mouse anti-mouse protein kinase Cα (PKCα) (1:100; Sigma-Aldrich); rabbit anti-mouse calbindin (1:100; Swant, Burgdorf, Switzerland); mouse anti-mouse rhodopsin (1:100; Abcam); rabbit anti-mouse glutamine synthetase GS (1:500; Sigma-Aldrich); goat anti-mouse glial fibrillary acidic protein (GFAP) (1:1000; Abcam); and goat anti-mouse Iba1 (1:100; Abcam). A blocking mouse on mouse commercial kit was used to avoid cross-reactivity when mouse-produced primary antibodies were used (Kit MOM TM, Vector Laboratories, Newark, USA). Primary antibodies were omitted in procedural negative controls. After washing in PBS, the retinas were incubated at 4°C overnight with the following secondary antibodies: anti-rat IgG-biotinylated (Abcam), anti-goat IgG-biotinylated (Santa Cruz Biotechnology), anti-rabbit and anti-goat Alexa Fluor 568 (Invitrogen, Carlsbad, CA, USA); anti-rabbit Alexa Fluor 488 (Abcam); anti-goat Alexa 488 (Thermo Fisher Scientific). Secondary antibodies were diluted at 1:100 in PBS. Streptavidin Alexa Fluor 488 (Invitrogen) or Streptavidin Alexa Fluor 568 (Invitrogen) were used as fluorochromes at 1:100 dilution. Nuclei were counterstained with Hoechst (Sigma-Aldrich) diluted in PBS at 1:100. Antifading media (Fluoromount, Sigma-Aldrich) was used for mounting slides before the analysis by laser scanning confocal microscope (TCS SP2 or TCS SP5; Leica Microsystems GmbH, Heidelberg, Germany).

2.5. Pericyte markers quantification

The expression of the specific pericyte markers NG2 and PDGF-Rβ was quantified in two-dimensional confocal microscopy images of immunohistochemically labelled whole-mount retinas from 5 Sirt1-tg and 5 wild type mice. Mean fluorescence intensity (MFI) values were obtained with the Leica LAS AF Lite imaging software (Leica) from two randomly selected areas per retina (Area NG2 = 0.06 mm^2; area PDGF-Rβ = 0.14 mm^2). Results are reported in Gray values, fluorescent intensity arbitrary units (AU). Acquisition parameters were maintained throughout the experiments, to ensure comparability across the different experiments.

2.6. Transmission electron microscopy (TEM)

Retinas were dissected into 1 mm^2 fragments, fixed in 2.5% glutaraldehyde and 2% paraformaldehyde (2 h at 4°C), and post-fixed in 1% osmium tetroxide. Next, samples underwent through a graded acetone series to dehydrate and were embedded in epoxy resin. Ultrathin sections (70 nm) were stained using lead citrate and 2% uranyl acetate. Sample examination was performed in a transmission electron microscope Jeol JEM-1400 (Jeol Ltd., Tokyo, Japan).

2.7. Scanning laser ophthalmoscopy (SLO)

Mice were anaesthetized by an intraperitoneal injection of a solution containing ketamine (12 mg/kg) and xylazine (100 mg/kg). Mydriasis was induced by topical administration of anaesthetic collyrium and tropicamide (Alcon, Barcelona, Spain). Eye moisture was prevented by continuous administration of Viscofresh (Allergan, Dublin, Ireland) on both eyes. Custom-made lenses were placed on the mouse corneas to enhance retinal vasculature visualization. Angiography was performed with HRA2 Imaging Instrument (Heidelberg Engineering, Heidelberg, Germany) after subcutaneous injection of 40 μl of 5% sodium fluorescein (Sigma- Aldrich). Retinal angiography was performed in both eyes of 6 Sirt1-tg and 5 WT mice. Superficial and deep vascular plexi were analysed in each eye.

2.8. Angiogenesis quantification

Angiogenesis was further determined by measuring morphological and spatial parameters of angiogenesis, including vascular density, lacunarity, and branching index. First, capillary density was measured in SLO retinal angiographies from 20 different eyes corresponding to 6 Sirt1-tg and 5 wild type mice by AngioTool software (Zudaire et al., 2011). Capillary density was analysed in 0.25 mm^2 areas at two depths corresponding to the superficial vascular plexus (SVP) and deep vascular plexus (DVP) in four different retinal regions: nasal superior, nasal inferior, temporal superior and temporal inferior.

Angiogenesis was further determined in microscopic images (200x magnification) of whole mount retinas immunostained with collagen IV from 5 different vascular areas at the deeper vascular plexus of each animal. AngioTool software was used to analyse morphological and spatial parameters of angiogenesis, including vascular density, lacunarity, and branching index in these micrographs.

2.9. Pericyte and endothelial cell number quantification

Retinal digest preparations of Sirt1-tg (n = 4) and wild type mice (n = 4) were analysed to determine numbers of pericytes and endothelial cells, as well as to quantify subpopulations of retinal pericytes. First, total numbers of pericytes and endothelial cells were counted in 5 randomly selected areas (magnification 400x). Numbers were standardized relative to the capillary area (number of cells per capillary area in arbitrary units). The ratio pericyte/endothelial cell was also determined by dividing the number of endothelial cells by pericytes in each retinal area. Subsequently, pericytes were divided into four subgroups according to the classification established by Pfister et al. (2008). Pericytes belonging to each subpopulation were counted in 5 to 10 randomly selected areas (magnification 400x).

2.10. Retinal digestion

Retinal digestion was performed as previously described (Kuwabara and Cogan, 1960; Hammes et al., 1991). Briefly, dissected retinas were fixed with neutral-buffered formalin, washed in filtered water and digested in a solution of 3% trypsin in 0.1 M Tris buffer (90 min at 37°C). Then, retinal blood vessels were isolated by several rinses in filtered water. Haematoxylin and PAS staining allowed blood vessel microscopy visualization (Nikon Eclipse E800; Nikon, Tokyo, Japan).

2.11. Basement membrane thickness quantification

Retinal basement membrane (BM) thickness was measured from transmission electron microscopy (TEM) images using Fiji (ImageJ, National Institutes of Health, USA). A total of six mice were analysed, including three SIRT1-overexpressing mice (Sirt1-tg) and three wild type (WT) controls. For each animal, five to seven retinal capillaries were examined. Morphometrical analyses were performed according to the circular grid intersection method, adapted from Siperstein et al. (1968). Briefly, this method utilized a circular grid with 16 equidistant radial divisions overlaid onto the image (Fig. 8C). BM thickness was recorded at each point where the radial lines intersected the basement membrane. This provided a systematic and evenly distributed sampling of the vessel. Unlike Siperstein et al. (1968), who excluded measurements when a radiating line intersected a pericyte, our study took into consideration measurements at sites containing pericytes. However, these measurements were taken specifically at the basement membrane located between the endothelial cell and pericyte, since the basement membrane between the pericyte and the surrounding tissue tends to be approximately twice as thick as other regions (Siperstein et al., 1968).

2.12. Statistical analysis

Results are shown as mean ± standard error of the mean (SEM). The statistical analyses of capillary density in SLO retinal angiographies of Sirt1-tg and wild type mice were performed using R software (Version 4.3.0, R Development Core Team), while graphical representations were generated with Prism software version 6 (GraphPad Software, Inc., La Jolla, CA, USA). Significance was accepted at $p < 0.05$. After checking the normal distribution of data with Shapiro-Wilk test, statistical analysis was performed using mixed linear models to evaluate the effect of strain, vascular plexus, and retinal quadrant on vascular density. Data included repeated measurements per eye, quadrant (temporal superior, nasal superior, temporal inferior, temporal inferior), and plexus (SVP, DVP), in both eyes of each animal, with individuals grouped by strain (Sirt1-tg, wild type). In this model, strain, plexus, quadrant, and interactions were considered fixed effects, and a random effect per animal was included to account for the dependence between measurements from the same subject. The eye was not explicitly modelled as a random effect, as no systematic differences or relevant contributions to variance were observed at that level. The significance of the fixed effects was evaluated using a type III ANOVA with freedom degree correction by the Kenward-Roger method. Since, a significant interaction between plexi and quadrants was detected, post-hoc comparisons adjusted by Tukey's method were performed.

The statistical analyses of SIRT1 relative mRNA expression, VEGF-A relative mRNA expression, VEGF-A_{164} relative mRNA expression, as well as pericyte markers area and cell number quantification were performed by unpaired *t*-test using Prism software. Graphical representation was also generated with Prism software. Significance was accepted at $p < 0.05$.

Finally, a linear mixed-effects model was fitted to assess differences in membrane thickness between wild type and Sirt1-tg mice. R software (Version 4.3.0, R Development Core Team) was used for statistical analysis, while graphical representations were generated with Prism software version 6 (GraphPad Software). The dependent variable was the measured thickness value. Fixed effect was Group (WT vs TG). Random intercepts were included for Mouse and Capillary to account for repeated measurements within the same animal and capillary. Estimated marginal means (EMMs) were computed using the emmeans package, and pairwise comparisons were performed with Tukey's adjustment for multiple testing. A p-value of <0.05 was considered statistically significant.

3. Results

3.1. Sirt1 expression in the retina of Sirt1-tg mice

Expression of Sirt1 was first analysed in the retina of Sirt1-tg mice to assess whether the upregulation of this gene was found in the retinal tissue. Quantitative RT-PCR indicated that Sirt1 mRNA transcript levels were increased in the retina of Sirt1-tg mice (2.8-fold; $p < 0.0001$; $n = 8$) (Fig. 1A). This increase in Sirt1 mRNA transcript levels was parallel to a similar increase in protein expression analysed by means of Western blot (Fig. 1B). Western blot experiments were performed using a pool of 6 retinas from 6 different Sirt1-tg and 6 different wild type animals. Therefore, although non quantifiable, they can be considered representative of the populations under study.

In addition, immunostaining of retinal paraffin-embedded sections with a specific anti-Sirt1 antibody confirmed the overexpression of Sirt1 throughout the retinal parenchyma (Fig. 1C). Subcellular localization of Sirt1 was predominantly nuclear, with a granular aspect and irregularly distributed within the nuclei. Higher immunoreactivity was observed in the ganglion cell and inner nuclear layers, in comparison with the inner and outer plexiform layers (Fig. 1D). In the outer nuclear layer, Sirt1 expression was confined to the scant cytoplasm surrounding the photoreceptor nuclei (Fig. 1C).

Previously, Jaliffa et al. (2009), showed that Sirt1 is exclusively nuclear in adult mouse retina, while Maloney et al. (2012) observed a cytoplasmic localization. During our observations, the granular aspect and irregular distribution of Sirt1 within the nuclei was consistent with the fact that Sirt1 is nuclear and can modulate chromatin function through direct deacetylation of histones (Zhang and Kraus, 2010), and that a large fraction of Sirt1 is associated with euchromatin (Michan and Sinclair, 2007). Furthermore, in addition to the Sirt1 cytoplasmic location in the outer nuclear layer, a slight Sirt1 expression was also detected in the inner and outer plexiform layers, where processes and synaptic contacts between neurons are located (Purves et al., 2004), thus confirming that Sirt1 could be also found in the cytoplasm of mouse retinal cells (Fig. 1D).

Cell-type overexpressing Sirt1 was also studied in paraffin-embedded sections by double immunohistochemistry with an anti-Sirt1 antibody and a variety of retinal cell markers: Brn3a, PKCα, calbindin, and rhodopsin (Filipek et al., 2003; Ohtoshi et al., 2004; Morona et al., 2008; Nadal-Nicolás et al., 2009). Double immunohistochemistry analysis showed that the overexpression of Sirt1 was found in the nuclei of ganglion, bipolar, and horizontal cells, and in the cytoplasm of rod photoreceptors (Supplementary Fig. 1).

Colocalization analyses with glial cell markers GS (Mizutani et al., 1998) and GFAP (Sarthy et al., 1991) revealed nuclear expression of Sirt1 in Müller cells and astrocytes, respectively (Supplementary Fig. 2A and B). Additionally, the use of the retinal microglia marker Iba1 (Ohsawa et al., 1997) demonstrated the overexpression of Sirt1 in the nuclei of this cell type (Supplementary Fig. 2C).

Sirt1 was also overexpressed in blood vessels of Sirt1-tg mice compared with wild type mice, as evidenced by collagen IV immunohistochemistry (Fig. 2A). Dual immunostaining with anti-Sirt1 antibody and the specific markers α-SMA, to label vascular smooth muscle cells and pericytes (Skalli et al., 1989), and CD34, to identify vascular endothelial cells (Pusztaszeri et al., 2006), confirmed that Sirt1 was specifically overexpressed in the nuclei of these cell types (Fig. 2B and C).

Altogether, these results showed that Sirt1-tg mice exhibit a moderate retinal Sirt1 overexpression, which is predominantly nuclear and found throughout the retinal parenchyma, including the nuclei of vascular retinal cells (endothelial cells, smooth muscle cells, and pericytes).

3.2. VEGF overexpression in the retina of Sirt1-tg mice

It has been stated that Sirt1 plays a dual role in neovascularization. Sirt1 promotes angiogenesis by inhibiting the DLL4-Notch signalling pathway and upregulating VEGFR-2 and VEGFR-3 (Wang et al., 2014), but it has been also demonstrated that Sirt1 overexpression suppresses HIF-1α mediated VEGF overproduction (Pan et al., 2020), thus reducing retinal angiogenesis (Cui et al., 2019; Wang et al., 2022; Law et al., 2024).

To unravel whether Sirt1 overexpression has a pro- or anti-angiogenic role in Sirt1-tg retinas, we investigated the expression of VEGF-A, the most potent inducer of retinal angiogenesis (Miller et al., 1994; Shibuya, 2008; Amadio et al., 2016). Total VEGF-A and, specifically VEGF-A_{164} mRNA transcript levels, the most prevalent isoform (Budd and Hartnett, 2010), were found increased by 1.5-fold ($p = 0.0022$; $n = 8$) and 5-fold ($p < 0.0001$; $n = 8$) respectively, in Sirt1-tg retinas (Fig. 3A). VEGF-A protein expression measured by Western blot analysis and quantified by densitometry was also increased by 1.8-fold in Sirt1-tg retinas, when compared with wild type (Fig. 3B). Western blot experiments were performed using a pool of 6 retinas from 6 different Sirt1-tg and 6 different wild type animals. Therefore, although non quantifiable, they can be considered representative of the populations under study.

Consistent with gene and protein overexpression, VEGF-A immunohistochemical analysis also showed an increase of expression

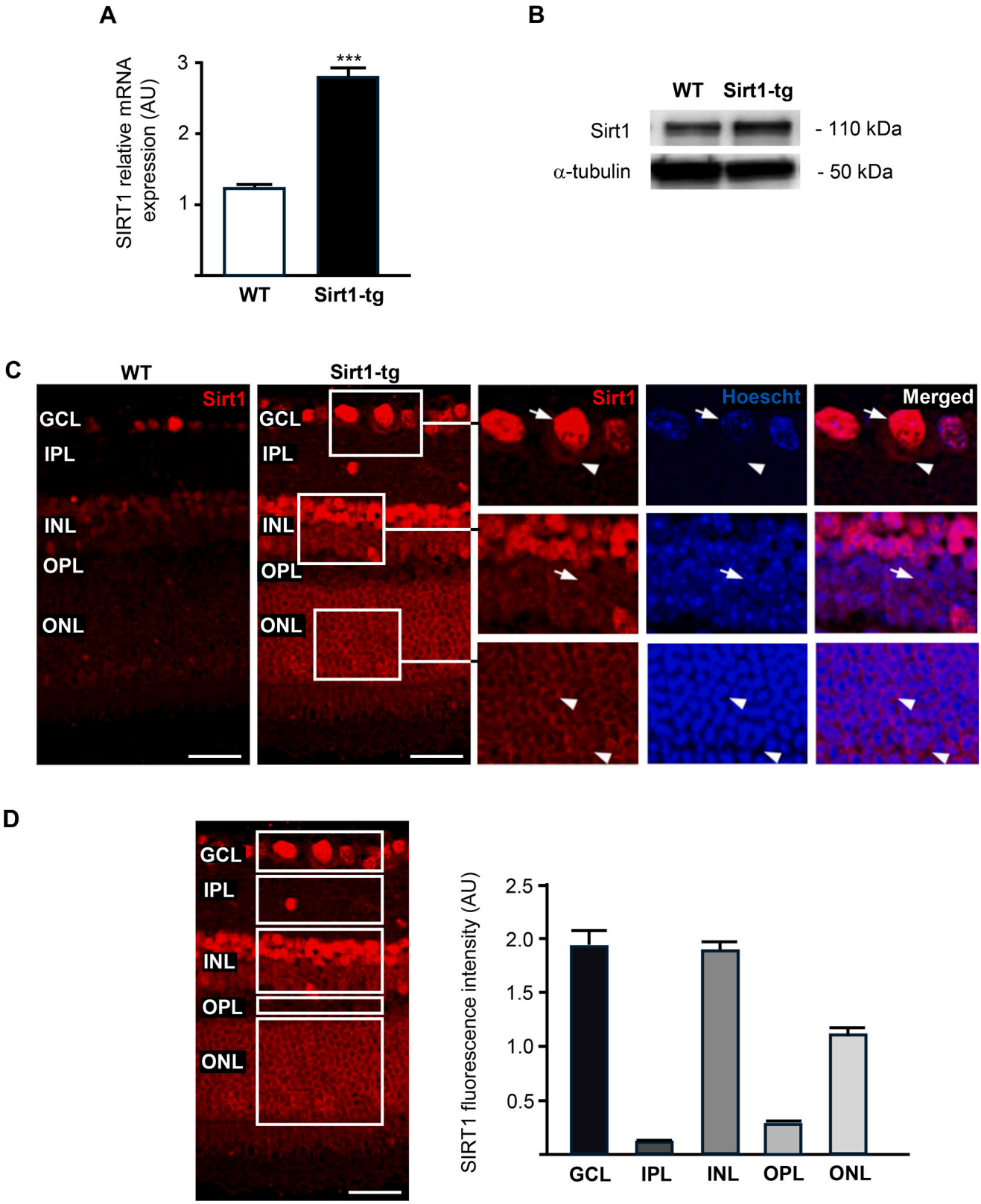


Fig. 1. Sirt1 overexpression in the retina of Sirt1-tg mice. (A) q-RT-PCR analysis showed increased Sirt1 mRNA transcript levels (2.8-fold) in Sirt1-tg retinas, after normalization with 36B4 housekeeping gene. Data are presented as mean ± SEM (n = 8). Asterisks indicate statistically significant differences: ***p < 0.001. (B) Western blot analysis also evidenced higher overexpression of Sirt1 in retinas of Sirt1-tg mice. α-tubulin was used as loading control. (C) Immunohistochemistry analysis confirmed the overexpression of Sirt1 (red) throughout the retinal parenchyma, primarily in the nucleus (arrow) but also in the cytoplasm (arrowhead) of retinal cells from Sirt1-tg mice. Nuclei were counterstained with Hoescht (blue) (D) Spatial distribution of Sirt1 expression was higher in the ganglion cell layer (1.9 ± 0.20 AU), inner nuclear layer (1.9 ± 0.12 AU), and outer nuclear layer (1.1 ± 0.06 AU), in contrast to the low expression observed in the outer plexiform layer (0.27 ± 0.04 AU) and inner plexiform layer (0.09 ± 0.04 AU). Data are presented as mean ± SEM (n = 5). AU: arbitrary units; GCL: ganglion cell layer; IPL: inner plexiform layer; INL: inner nuclear layer; OPL: outer plexiform layer; ONL: outer nuclear layer. Scale bar: C (WT) = 31.51 μm; C (Sirt1-tg) = 30.41 μm; D = 30.41 μm.

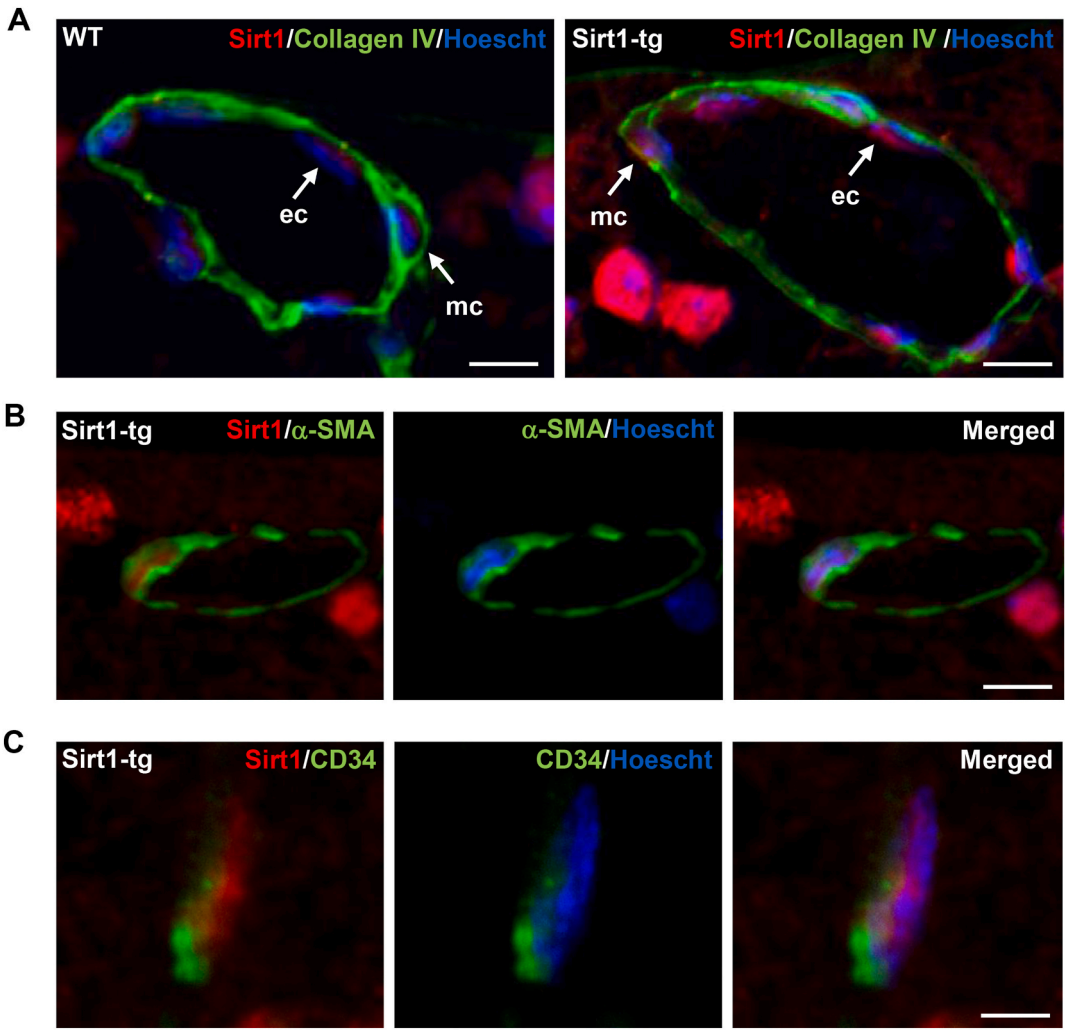


Fig. 2. Sirt1 overexpression in retinal blood vessels of Sirt1-tg mice. (A) Retinal sections immunostained with anti-collagen IV (green) showed increased expression of Sirt1 (red) in retinal vascular cells of Sirt1-tg mice. (B) Dual immunolabeling with α-SMA (green) and Sirt1 (red) confirmed that mural cells overexpressed Sirt1 in their nuclei. (C) Dual immunolabeling with CD34 (green) and Sirt1 (red) confirmed that endothelial cells overexpressed Sirt1 in their nuclei. Nuclei were counterstained with Hoechst (blue). ec: endothelial cell; mc: mural cell. Scale bars: A (WT) = 9.47 μm; A (Sirt1-tg) = 8.52 μm; B = 10.29 μm; C = 6.09 μm.

throughout the retinas of Sirt1-tg mice (Fig. 3C). The outer nuclear layer was the only retinal layer practically devoid of VEGF-A expression (Fig. 3C). Thus, our results showed that Sirt1 overexpression induces VEGF-A expression in the retina of Sirt1-tg mice.

3.3. Angiogenesis was not increased in the retina of Sirt1-tg mice

After establishing a correlation between Sirt1 and VEGF-A overexpression, we asked if retinal blood vessels from Sirt1-tg mice respond to VEGF-A upregulation by producing new vessels. For this purpose, capillary density was measured in SLO retinal angiographies from 20 different retinas from 6 Sirt1-tg and 5 wild type mice (Fig. 4A). Previous results from our laboratory have demonstrated that vascular densities significantly differ between plexuses and hemispheres in C57Bl6 wild type mice (McLenachan et al., 2015). Therefore, to avoid misinterpretation of results, eight areas corresponding to the inferior-nasal, superior-nasal, inferior-temporal and superior-temporal regions of SVP and DVP were selected in each retinal angiography for microvessel density analysis (Fig. 4A). No significant differences ($p = 0.688$) were found between wild type and Sirt1-tg retinas when comparing vascular density of the different areas selected (SVP inferior-nasal: 37.10 ± 2.907% vs 35.08 ± 1.548%; SVP superior-nasal: 32.48 ± 1.837% vs 38.44 ± 1.646%; SVP inferior-temporal: 34.81 ± 2.172% vs 35.08 ± 1.5%; SVP superior-temporal: 30.67 ± 2.292% vs 33.98 ± 2.13%; DVP inferior-nasal: 37.49 ± 2.343% vs 36.49 ± 3.072%; DVP superior-nasal: 3.04 ± 1.615% vs 43.43 ± 0.808%; inferior-temporal: 38.71 ± 2.609% vs 40.46 ± 1.694%; superior-temporal: 45.68 ± 1.474% vs 42.68 ± 2.104%) (Fig. 4B). Confirming our previous results (McLenachan et al., 2015), only a statistically significant increase of vascular density in the DVP compared to the SVP was found (41.10 ± 0.89% vs 34.8 ± 0.887%; $p < 0.0001$) regardless of whether the mouse was Sirt1-tg or wild type.

Morphological and spatial parameters of angiogenesis, including vascular density, lacunarity, and branching index were more thoroughly measured by using the AngioTool software (Zudaire et al., 2011) in confocal laser microscopy images of whole mount retinas immunostained with anti-collagen type IV antibody ($n = 5$ retinas from 5 different animals per group) (Fig. 5A). No significant differences ($p = 0.8310$) were found when comparing vascular density between wild type and Sirt1-tg retinas (37.84 ± 1.594% vs 38.27 ± 1.206%) (Fig. 5B). Quantification of branching index, which provides a measurement of the sprouting activity during angiogenesis (Zudaire et al., 2011), was also unable to detect statistically significant differences ($p = 0.5368$) between wild type and Sirt1-tg mice (3.992 ± 0.3503 arbitrary units (AU) vs 4.243 ± 0.221 AU) (Fig. 5C). Finally, we analysed the lacunarity parameter which is used to measure spatial dispersion of

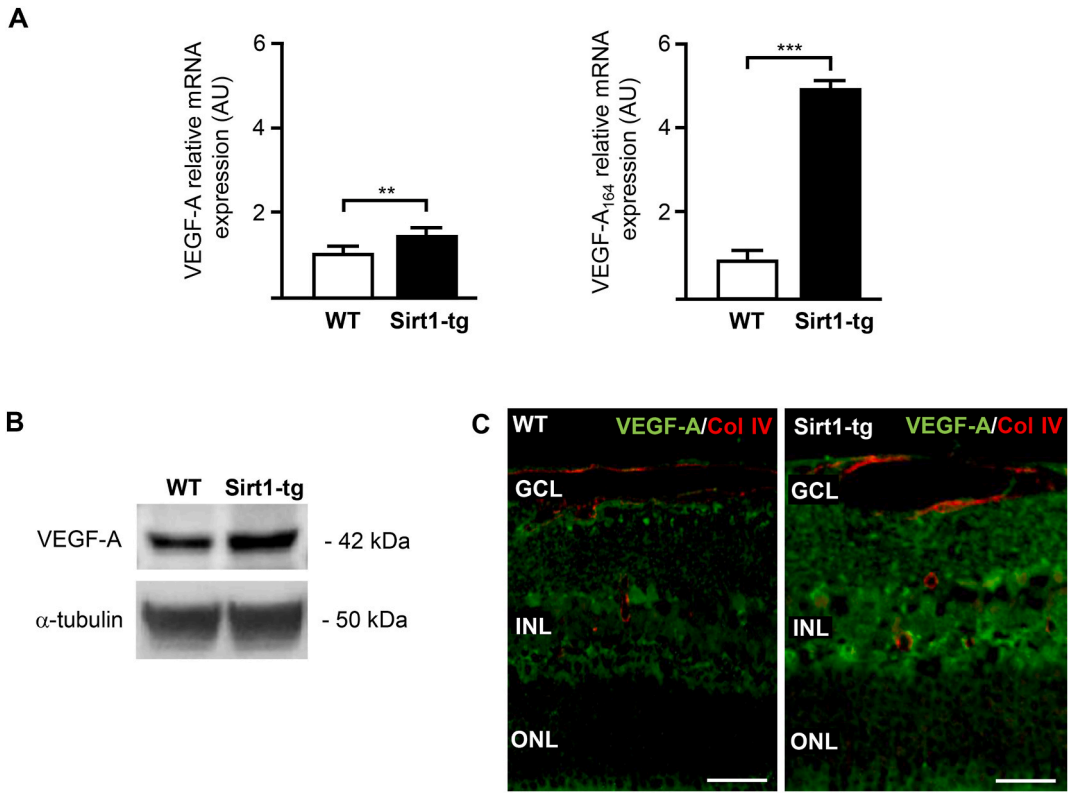


Fig. 3. VEGF overexpression in the retina of Sirt1-tg mice. (A) Sirt1-tg mice showed increased mRNA transcript expression of VEGF-A by 1.5-fold ($p = 0.0022$; $n = 8$), along with a 5-fold ($p < 0.0001$; $n = 8$) increase of specific proangiogenic factor VEGF-A_{164} mRNA transcript expression, compared with wild type retinas, after normalization with 36B4 housekeeping gene. Data are presented as mean ± SEM ($n = 8$). (B) Western blot analysis revealed a significant increase of VEGF-A protein expression in Sirt1-tg retinas, consistent with higher intensity of the 42 kDa band. α-tubulin was used as a loading control. (C) Accordingly, retinal sections immunostained with anti-VEGF-A antibody (green) and anti-collagen IV antibody (red), revealed VEGF-A overexpression throughout the retinal parenchyma of Sirt1-tg mice, when compared with wild type. AU: arbitrary units; Col IV: collagen IV. Asterisks indicate statistically significant differences: **$p < 0.01$; ***$p < 0.001$. Scale bars: C (WT) = 30.82 μm; C (Sirt1-tg) = 22.27 μm.

blood vessels (Tălu et al., 2015). Our results showed no significant differences ($p = 0.8672$) in the average lacunarity of the retinal vasculature (Fig. 5D), confirming that retinal blood vessel spatial organization is similar in wild type and Sirt1-tg mice, with no evidence of changes in lacunarity that frequently occur during angiogenesis (0.1579 ± 0.012 AU vs 0.1555 ± 0.008 AU) (Zudaire et al., 2011). Altogether, these results showed that although VEGF-A expression is elevated in retinas overexpressing Sirt1, there is no evidence of increased angiogenesis in them.

3.4. *PDGF-B/PDGFR-β pathway activation and increased pericyte coverage but not pericyte recruitment in the retina of Sirt1-tg mice*

After verifying that there were no signs of increased angiogenesis in the retina of Sirt1-tg mice during VEGF-A upregulation, we next investigated key factors that can counteract new vessel formation through induction of blood vessel stability, such as the recruitment of pericytes into the vessel wall and basement membrane deposition (Armulik et al., 2005; von Tell et al., 2006).

PDGF-B/PDGFR-β signalling pathway plays a critical role in pericyte recruitment (Armulik et al., 2005; Andrae et al., 2008; Gaengel et al., 2009). PDGF-B is secreted by endothelial cells and binds to its receptor PDFGR-β on the surface of pericytes inducing pericyte migration towards endothelial tube and vascular stabilization (Lindahl et al., 1997; Armulik et al., 2005, 2011; Kofler et al., 2011). Therefore, the expression of PDGF-B was assessed by means of Western blot analysis as shown in Fig. 6A. Retinas of Sirt1-tg mice presented an elevation of PDGF-B protein expression (1.7-fold), when compared with wild type retinas. PDFGR-β protein levels, which were also analysed by Western blot analysis, increased (1.4-fold) in Sirt1-tg retinas (Fig. 6B). Western blot experiments were performed using a pool of 6 retinas from 6 different Sirt1-tg and 6 different wild type animals. Therefore, although non quantifiable, they can be considered representative of the populations under study. These results suggest that PDGF-B/PDGFR-β signalling pathway is increased in the retinal blood vessel of Sirt1-tg mice, thus suggesting that pericyte recruitment and vessel stabilization may be also increased.

Pericytes exhibit remarkable heterogeneity in terms of protein expression and morphology (Hughes and Chan-Ling, 2004; Armulik et al., 2005). Therefore, to avoid misleading results, we relied on a combination of methods to differentiate retinal pericytes, including specific immunostaining with two validated pericyte markers PDGFR-β (Lindahl et al., 1997) and NG2 (Ozerdem et al., 2001).

To assess if the increase of PDGF-B/PDGFR-β induced pericyte recruitment in the retinal blood vessels of Sirt1-tg mice, double immunostaining with anti-PDGFR-β and anti-collagen type IV antibody was used. Our results evidenced higher fluorescence intensity of PDGFR-β within the vessel wall, revealing a statistically significant ($p = 0.0495$) increased expression of PDGFR-β per vessel area in Sirt1-tg mice, when compared to wild type mice (34.54 ± 3.413 AU vs 25.74 ± 1.596 AU; $n = 6$ retinas from 6 different animals per group) (Fig. 6C). Accordingly, whole mount retinas immunostained with anti-NG2 antibody and anti-collagen type IV showed a significant increase in the expression of NG2 per vessel area in the capillaries of Sirt1-tg mice when compared to wild type mice (0.7929 ± 0.06993 AU vs 0.2889 ± 0.07427 AU; $n = 5$ retinas from 5 different animals per group; $p < 0.0002$) (Fig. 7A). Given that NG2 and PDGFR-β essentially mark the cytoplasm and cytoplasmic membrane of pericytes (Mai-Morente et al., 2021), these results

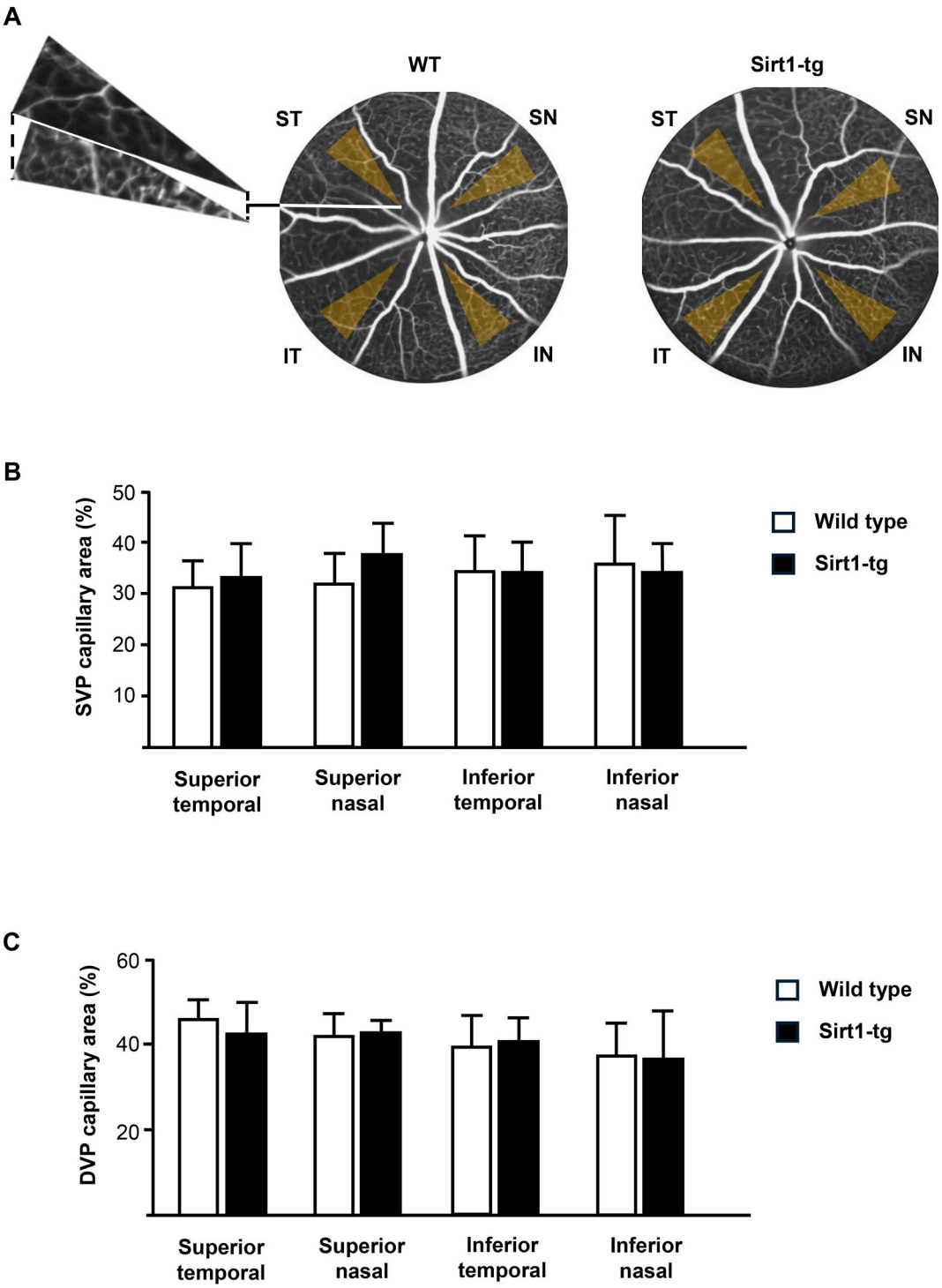


Fig. 4. In vivo quantification of the capillary density. (A) Microvessel density was assessed in both the superficial and deep vascular plexi in four selected areas of the retinal parenchyma (yellow). (B) Bar graphs show no differences in capillary density between wild type and Sirt1-tg mice in the superficial vascular plexus (SVP) (inferior-nasal: 37.10 ± 2.907% vs 35.08 ± 1.548%; superior-nasal: 32.48 ± 1.837% vs 38.44 ± 1.646%; inferior-temporal: 34.81 ± 2.172% vs 35.08 ± 1.5%; superior-temporal: 30.67 ± 2.292% vs 33.98 ± 2.13%; n = 5 wild type and 6 Sirt1-tg mice). (C) No differences were found in capillary density either in the deep vascular plexus (DVP) between wild type and Sirt1-tg mice (inferior-nasal: 37.49 ± 2.343% vs 36.49 ± 3.072%; superior-nasal: 3.04 ± 1.615% vs 43.43 ± 0.808%; inferior-temporal: 38.71 ± 2.609% vs 40.46 ± 1.694%; superior-temporal: 45.68 ± 1.474% vs 42.68 ± 2.104%; n = 5 wild type and 6 Sirt1-tg mice). WT: wild type; ST: superior-temporal; SN: superior-nasal; IT: inferior-temporal; IN: inferior-nasal.

indicated that Sirt1 increases pericyte vessel coverage.

It is known that the expression of pericyte markers varies along pericyte development, during pathological processes, and in cell culture (Zhu et al., 2022). According to this, NG2 expression is downregulated in mature, quiescent vasculature, but is upregulated during vascular remodelling or induced neovascularization (Stallcup, 2018). Therefore, we cannot rule out the possibility of an increase in the expression of NG2 in Sirt1-tg mice mediated by VEGF-A. To confirm whether Sirt1 over-expression induced pericyte increased expression of NG2 or increased pericyte recruitment, the number of pericytes standardized to vessel

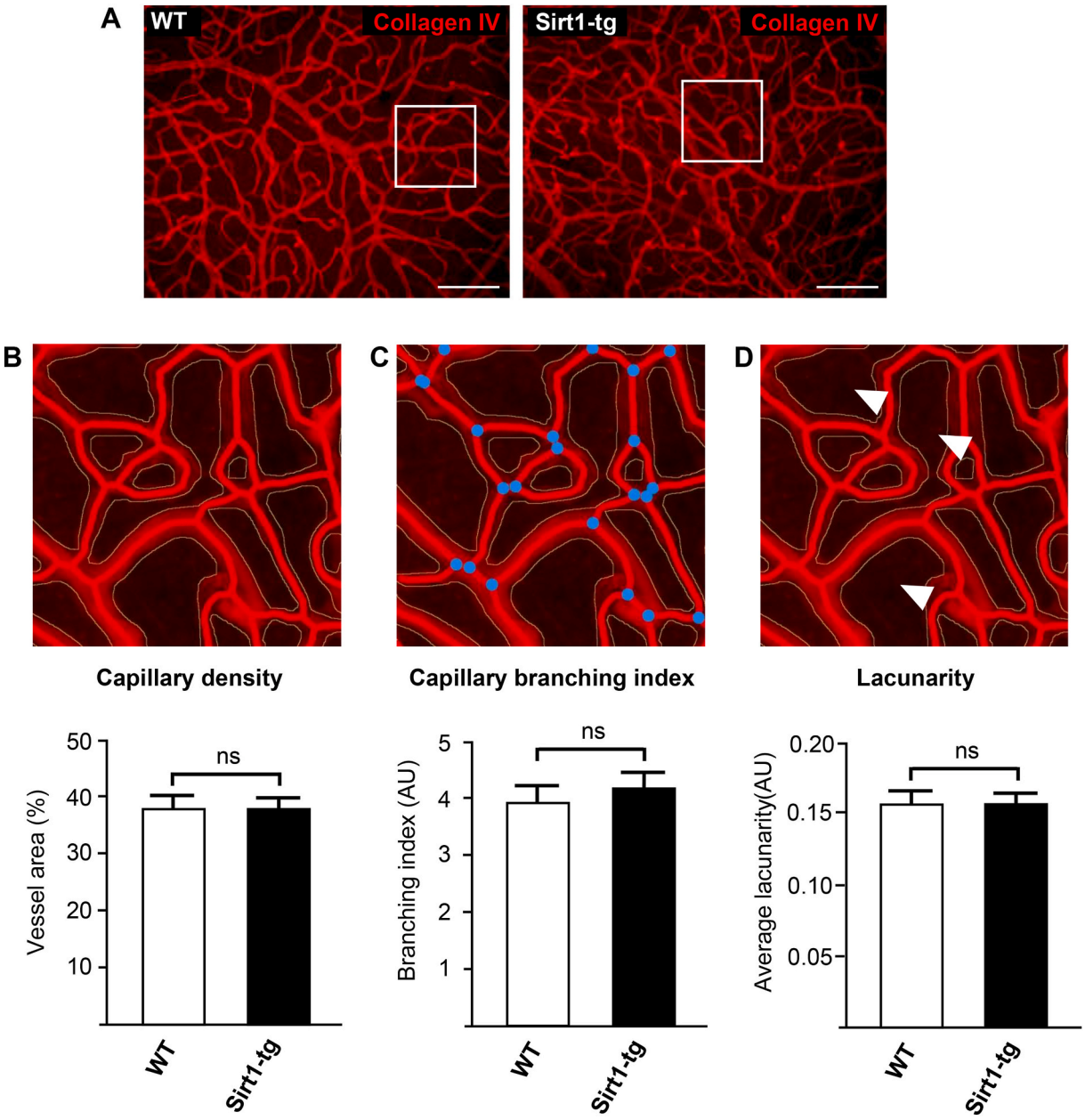


Fig. 5. Angiogenic parameters were not increased in the retina of Sirt1-tg mice. (A) Quantitative analysis of angiogenesis was performed using whole mount retinas immunostained with anti-collagen IV antibody (red) to label the retinal blood vessels to measure angiogenic parameters with the AngioTool software. (B) Retinal capillary density was obtained by calculating the percentage of blood vessel area skeletonized (red) per image. Compared to wild type, Sirt1-tg retinas did not show significant differences of vascular density (37.84 ± 1.594% vs 38.27 ± 1.206%, n = 5). (C) Capillary branching index measured the number of vessel junctions represented by branching points (blue) at the confluence of more than two vessel segments, normalized per unit area of retina. No significant differences were observed between wild type and Sirt1-tg retinas (3.992 ± 0.3503 AU vs 4.243 ± 0.2206 AU; n = 5). (D) Capillary lacunarity parameter, used to assess the non-vascular space surrounding blood vessels (arrowheads) showed no significant differences in Sirt1-tg retinas in comparison with wild type (0.1579 ± 0.01209 AU vs 0.1555 ± 0.007553 AU; n = 5). Data presented as mean ± SEM (n = 5). AU: arbitrary units; ns: not significant. Scale bars: 72.85 μm.

area was quantified in trypsin-digested Sirt1-tg and wild type retinas (Fig. 8A). No significant differences (p = 0.1693) were found when comparing the pericyte number between wild type and Sirt1-tg retinas (1466 ± 0,07401 pericytes vs 1338 ± 0,05538 pericytes; n = 4 retinas from 4 different animals per group) (Fig. 8B).

Four types of pericytes have been identified in the retina: type I pericytes are located on straight capillaries with broad contact to the underlying endothelium, type II pericytes are situated in capillary branches, type III pericytes have triangular nuclei and are attached to intercapillary fibrous strands, and type IV pericytes are located into intercapillary fibrous strands (Pfister et al., 2008). Given that the response of pericytes to Sirt1 overexpression may differ for distinct subpopulations, pericyte subpopulations were quantified in trypsin-digested retinas from Sirt1-tg and wild type mice (Supplementary Fig. 3A). The count of pericyte subpopulations in relation to the total number of pericytes showed that the distribution of the four types of pericytes was completely unaffected in Sirt1-tg retinas (Supplementary Fig. 3B). According to all these data, it is safe to assume that Sirt1 overexpression induced increased pericyte coverage without pericyte recruitment.

NG2 acts as a crucial regulator of vascular maturation, stability, and remodelling. It promotes pericyte-endothelial cell crosstalk, essential for

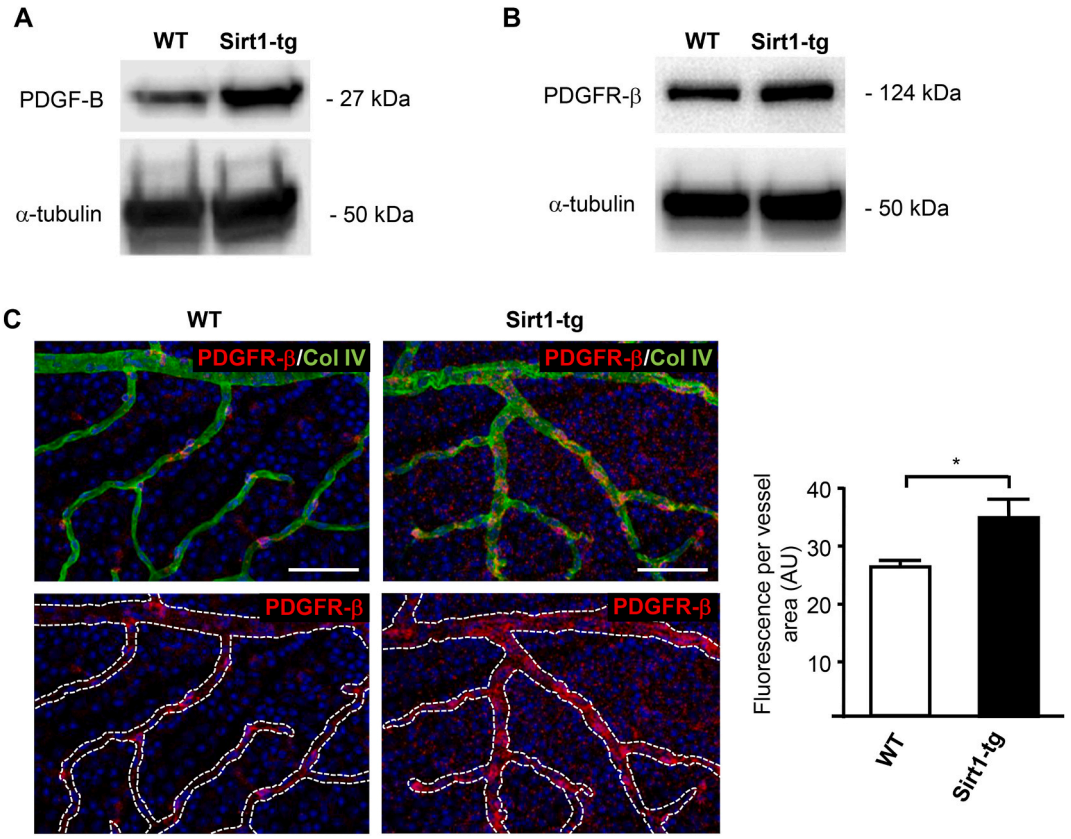


Fig. 6. PDGF-B/PDGFR-β pathway activation and increased pericyte coverage in the retina of Sirt1-tg mice. Western blot analysis revealed a significant increase of PDGF-B (A) and PDGFR-β (B) protein expression in Sirt1-tg retinas, compared to wild type. α-tubulin was used as a loading control. Consistently, the pericyte marker PDGFR-β (red) was also increased within retinal capillaries immunostained with collagen IV (green) in Sirt1-tg retinas compared with wild-type (25.74 ± 1.596 AU vs 34.54 ± 3.413 AU) (n = 6). Nuclei were counterstained with Hoechst (blue). Data are presented as mean ± SEM. Asterisks indicate statistically significant differences: *p < 0.05. WT: wild type; AU: arbitrary units; Col IV: collagen IV. Scale bars: WT = 63.14 μm; Sirt1-tg = 52.61 μm.

vessel stabilization, basement membrane assembly, and maintaining blood-brain barrier integrity (Huang et al., 2010; You et al., 2014). Therefore, our results suggest that VEGF-driven angiogenesis might be prevented by vessel stabilization processes such as increased pericyte coverage and increased NG2 expression.

3.5. Endothelial cell number did not increase in Sirt1-tg mice

VEGF acts as a signalling molecule, binding specific receptors on endothelial cells to promote their growth, migration, and survival, thus driving angiogenesis (Leung et al., 1989; Keck et al., 1989; Lee et al., 2025). In addition, it has been shown that NG2 expressed by pericytes can promote endothelial cell proliferation and migration (Chekenya et al., 2002; Fukushi et al., 2004). According to this, the effect of Sirt1 overexpression was also assessed in vascular endothelial cells of Sirt1-tg and wild type mice trypsin-digested retinas (Fig. 8A). No significant differences between wild type and Sirt1-tg mice could be detected neither in endothelial cell number (32.30 ± 1.307 endothelial cells vs 31.47 ± 1.364; p = 0.6608 endothelial cells; n = 4 retinas from 4 different animals per group) (Fig. 8C) nor in the endothelial to pericyte ratio (3.773 ± 0.1468 AU vs 3.558 ± 0.1559 AU; p = 0.3179; n = 4 retinas from 4 different animals per group) (Fig. 8D). Therefore, our results indicated that Sirt1-induced VEGF and NG2 overexpression did not trigger proliferation or migration of retinal endothelial cells.

3.6. Blood vessel basement membrane is altered in Sirt1-tg mice

Blood vessel basement membrane deposition, a critical step in vessel maturation, has been shown to be highly dependent on pericytes NG2 expression as this proteoglycan acts as cell surface ligand for collagen IV (Huang et al., 2010). Therefore, we aimed to investigate whether Sirt1-induced NG2 overexpression affected collagen IV deposition in Sirt1-tg mice. As expected, Western blot analysis revealed that collagen IV expression was significantly increased in Sirt1-tg retinas (Fig. 9A). Western blot experiments were performed using a pool of 6 retinas from 6 different Sirt1-tg and 6 different wild type animals. Therefore, although non quantifiable, they can be considered representative of the populations under study.

To analyse if increased collagen IV was accompanied by an actual basement membrane thickening, capillary basement membrane thickness was studied by electron transmission microscopy in 3 WT and 3 Sirt1-tg mice (5 to 7 different capillaries per animal were measured) (Fig. 9B). Contrary to expectations, an apparent decrease in basement membrane thickness was observed in Sirt1-tg mice when compared to WT (Fig. 9B). Morphometrical analysis according to the method proposed by Siperstein and colleagues (1968), confirmed a significant decrease in basement membrane thickness in retinal capillaries of Sirt1-tg mice (WT = 0.137 ± 0.10 μm vs Sirt1-tg = 0.100 ± 0.10 μm; p = 0.047; n = 3 animals per group, 5-7 capillaries per animal) (Fig. 9C). However, the analysis of blood vessel basement membrane under transmission electron microscopy showed an increase in the electron density of the *lamina densa* in the capillary basement membrane of Sirt1-tg mice (Fig. 9B). Collagen IV is exclusively found in the *lamina densa* of basement membranes (Adachi et al., 1997). Therefore, this increase in electron density may reflect the collagen IV overexpression observed in Western blot experiments.

Furthermore, immunohistochemistry in whole mount retinas evidenced the exact location of collagen IV, revealing focal areas of

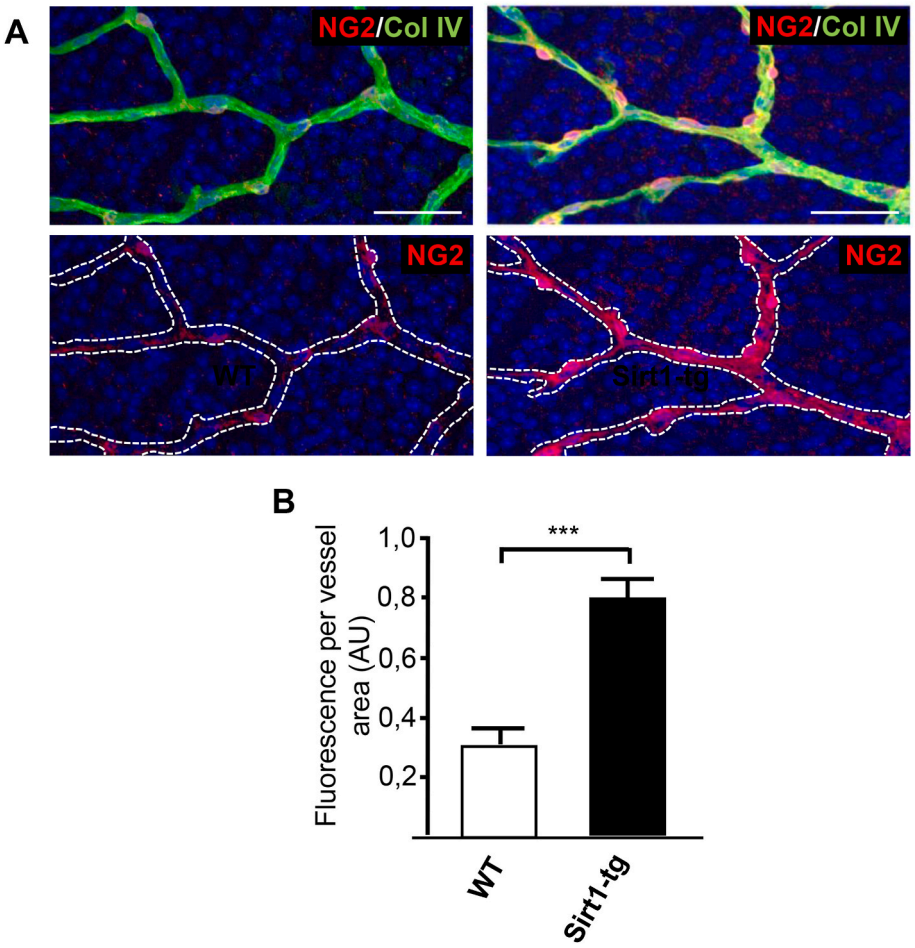


Fig. 7. Increased NG2 expression in the retina of Sirt1-tg mice. (A) NG2 expression was analysed in whole mount retinas immunostained with anti-NG2 antibody (red) to label pericytes and anti-collagen type IV antibody (green) to evidence the vascular basement membrane. (B) The quantification of fluorescence intensity evidenced a significant increase in the expression of NG2 standardized to the capillary area in Sirt1-tg retinas when compared with wild type retinas (0.2889 ± 0.07427 AU vs 0.7929 ± 0.06993 AU) (n = 5). Nuclei were counterstained with Hoechst (blue). Data are presented as mean ± SEM. Asterisks indicate statistically significant differences: ***p < 0.001. AU: arbitrary units; Col IV: collagen IV. Scale bars: WT = 54.96 μm; Sirt1-tg = 51.98 μm.

increased collagen IV fluorescence intensity in Sirt1-tg capillaries (Fig. 9D). Thus, our results indicated not a general increase in collagen IV expression and deposition, but an overexpression restricted to focal areas of the capillary network. Collagen IV synthesis and deposition provide a scaffold indispensable for vascular survival and maturation (Bonanno et al., 2000; Bahramsoltani et al., 2014). Therefore, our results suggest that Sirt1 overexpression induces collagen IV deposition in specific areas of the basement membrane in an attempt to stabilize retinal blood vessels in Sirt1-tg mice.

4. Discussion

Among sirtuins, Sirt1 is considered the most critical regulator of vascular homeostasis and diseases through its action at multiple cellular levels (D'Onofrio et al., 2015). Recently, the prominent role of Sirt1 in the regulation of vascular retinopathies is recognized by the fact that diabetic mice overexpressing Sirt1 are protected against the development of degenerative retinal capillaries (Mishra et al., 2018). Furthermore, an intravitreal injection of AAV2-Sirt1 has been proved to reverse the formation of acellular capillaries in db/db mice (Adu-Agyeiwaah et al., 2023). However, despite this evidence, the exact mechanism underlying the vascular protective role of Sirt1 in vascular disease is not fully understood.

According to our results, Sirt1 promotes VEGF-A overexpression. Although VEGF-A is the most well-established angiogenic factor, our results also showed that Sirt1-induced VEGF-A overexpression did not trigger increased vessel formation in the retinas of Sirt1-tg mice. The angiogenic activity of Sirt1 has been well illustrated in several previous studies (Potente et al., 2007; Law et al., 2024). However, Sirt1 could play a dual role in angiogenesis since it can induce angiogenesis but also can suppress stress-induced pathological angiogenesis (Law et al., 2024). In this regard, it has been reported that elevated levels of Sirt1 promote revascularization by modulating the expression of angiogenic factors in ischemic retinas (Chen et al., 2013). Similarly, Sirt1 activation by resveratrol has been demonstrated to significantly elevate VEGF levels on focal cerebral ischemic injury (Dong et al., 2008). By contrast, it has been also demonstrated that, during hypoxia, Sirt1 diminishes HIF-1α acetylation and blocks the endothelial tube formation in hypoxia-conditioned media (Lim et al., 2010).

Angiogenesis is a multi-step process by which endothelial cells generate a new functional blood vessel, including the production of proteases, migration of tip cells, and lumen formation (Dudley and Griffioen, 2023). These newly formed vessels are extremely unstable, so they undergo a stage of maturation which involves pericyte recruitment and basement membrane deposition (Jain, 2003). Pericyte covering has been directly implicated in leading capillary resistance to regression in vivo (Ribatti et al., 2011). By contrast, lack of pericyte recruitment leads to endothelial hyperplasia and increased vascular permeability. Thus, connecting pericytes with vessel stability and maturation (Stapor et al., 2014). PDGF-B/PDGFR-β signalling pathway

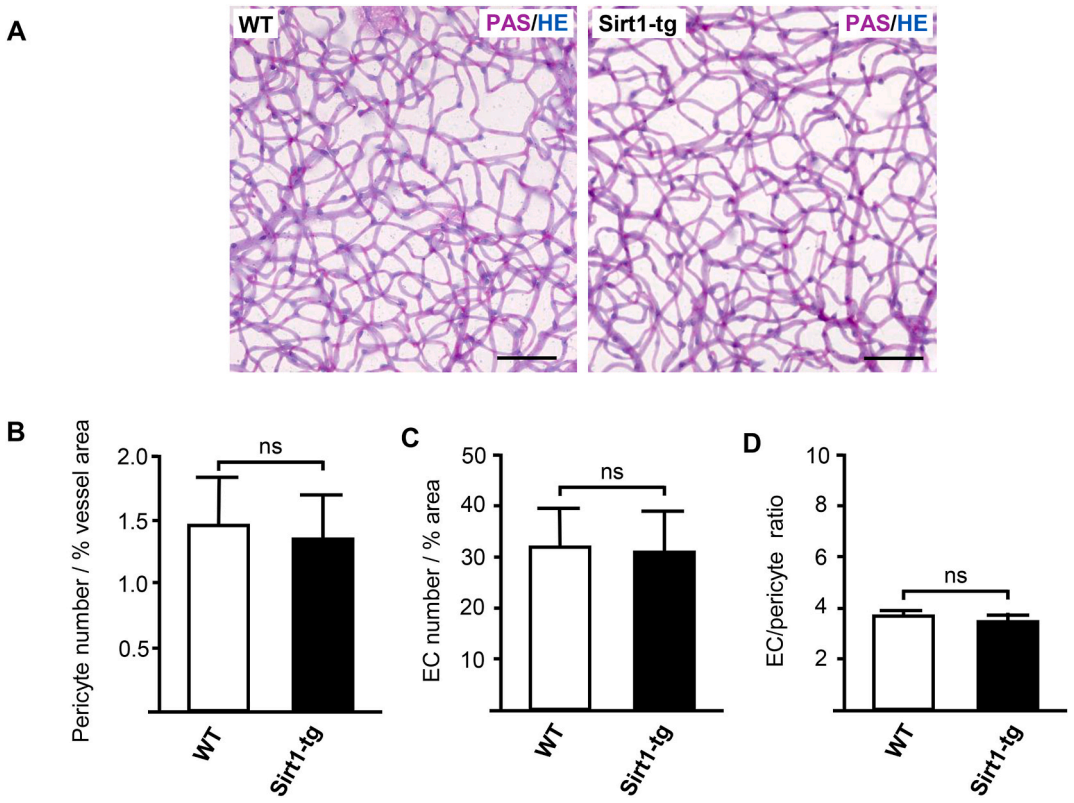


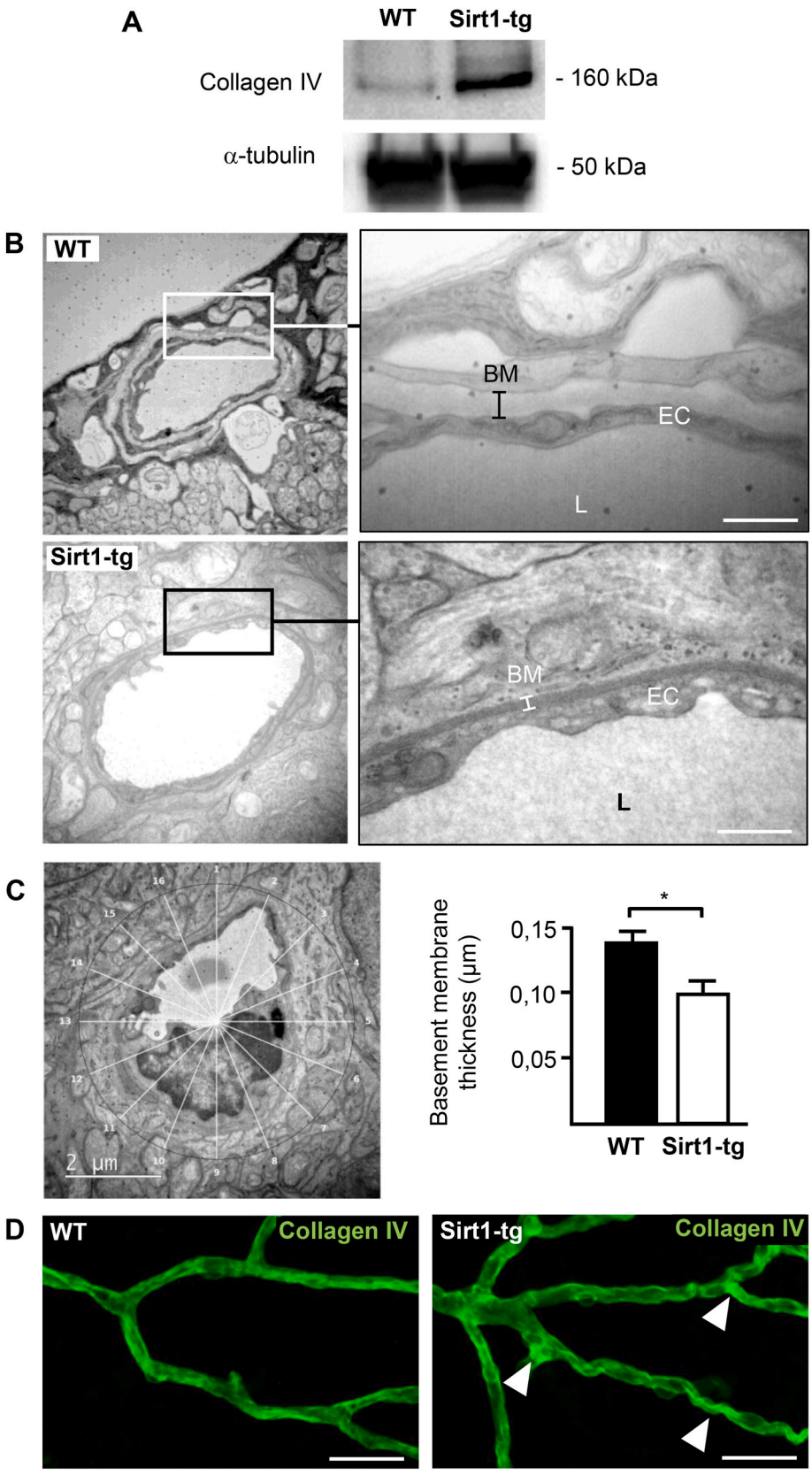
Fig. 8. Pericyte and endothelial cell number were not increased by Sirt1 overexpression. (A) PAS-Haematoxylin (PAS/HE) stained trypsin-digested retinas were used to quantify the total number of pericytes and endothelial cells standardized to vessel area. (B) No differences in pericyte number were found between Sirt1-tg and wild type retinas (1.466 ± 0.07401 pericytes vs 1.338 ± 0.05538 pericytes; p = 0.163) (n = 4). (C) No changes were observed either in the number of endothelial cells between Sirt1-tg and wild type retinas (32.30 ± 1.307 endothelial cells vs 31.47 ± 1.364 endothelial cells; p = 0.6608; n = 4). (C) Accordingly, endothelial cell/pericyte ratio did not vary between groups (3.773 ± 0.1468 vs 3.558 ± 0.1559; p = 0.3179; n = 4). Data presented as mean ± SEM. ns: not significant; EC: endothelial cell. Scale Bar: A = 64.61 μm.

plays a key role in the recruitment of mural cells. PDGF-B secreted by endothelial cells interact in a paracrine manner with PDGFR-β expressed by pericytes. Thus, promoting pericyte proliferation and migration (Hellström et al., 1999; Betsholtz, 2004). PDGF-B or PDGFR-β deficiency in mice is associated with reduced pericyte coverage in various organs, leading to microvascular leakage, endothelial cell over-proliferation, and impaired blood flow (Benjamin et al., 1998; Betsholtz, 2004; Geevarghese and Herman, 2014). More concretely, in the retina, endothelium-restricted PDGF-B conditioned knockouts, with more than 50% pericyte loss, developed lesions similar to diabetic proliferative retinopathy (Enge et al., 2002). According to authors, pericyte deficiency initially triggered vascular regression of the deep vascular plexus resulting in retinal hypoxia and vessel proliferation in the superficial vascular plexus (Enge et al., 2002). According to these data, our results showed that in a proangiogenic state mediated by VEGF-A, angiogenesis may be prevented in Sirt1-tg mice retinas by upregulation of the PDGF-B/PDGFR-β signalling pathway and increased pericyte coverage.

NG2 is expressed by microvascular pericytes in newly formed blood vessels (Ozerdem et al., 2001) and is considered a key factor in the development of a functional vasculature (Huang et al., 2010). It has been documented that NG2 is able to promote angiogenesis by enhancing endothelial cell migration and morphogenesis (Fukushi et al., 2004). However, studies on NG2 null mice have also demonstrated that NG2 contributes to vessel maturation by promoting pericyte recruitment, pericyte ensheathment, pericyte-endothelial cell interactions, pericyte maturation, and basement membrane collagen IV deposition (Huang et al., 2010). Our results indicated that Sirt1 overexpression is able to induce an increased expression of NG2 along with increased pericyte coverage and focal areas of increased collagen IV deposition. These NG2 overexpression may act agonistically with increased PDGF-B/PDGFR-β signalling, stabilizing blood vessels and modulating the proangiogenic effect of VEGF overexpression.

The pathological functions of VEGF-A in neovascular ocular diseases have been well established. In humans, high levels of VEGF-A expression have been correlated with neovascularization during age related macular degeneration (Kvanta et al., 1996; Rakic et al., 2003), diabetic retinopathy, and other retinal disorders (Aiello et al., 1994; Adamis et al., 1994). However, it is currently known that VEGF exerts protective roles in neurons and endothelial cells. In this regard, it has been demonstrated that VEGF-A directly prevents retinal ganglion cells apoptosis through phosphoinositide-3-kinase (PI3K)/Akt signalling in mouse models of acute toxicity and hypertensive glaucoma (Foxton et al., 2013). In addition, VEGF produced by pericytes may act in a juxtacrine/paracrine manner as a stabilizing factor for endothelial cells (Ribatti et al., 2011). Moreover, it has been shown that continuous expression of VEGF by endothelial cells is needed to sustain vascular integrity and cellular viability. Mice deletion in the endothelial compartment results in vascular degeneration and premature death from strokes and haemorrhages (Lee et al., 2007). Autocrine function of endothelial cell VEGF promotes endothelial cell survival by regulation of metabolism and autophagy through regulation of FOXO1 (Domigan et al., 2015) and prevents apoptosis through PI3/Akt pathway (Gerber et al., 1998). Thus, we postulate that Sirt1 overexpression could induce a moderate and controlled VEGF response able to promote protective effects on vascular and neuronal retinal cells while preventing angiogenesis through vessel stabilization mechanisms.

To analyse the effects of Sirt1 in the retinal vasculature, we used a mouse model with moderate Sirt1 overexpression generated by using a transgene construct containing the complete Sirt1 gene and the adjacent Dnajc12 gene that codes for a heat shock protein of the Hsp 40 family



(caption on next page)

Fig. 9. Blood vessel basement membrane was altered in the retina of Sirt1-tg mice. (A) Western blot analysis of Collagen IV, a specific component of the retinal blood vessel basement membrane, showed an increased expression of this protein in Sirt1-tg retinas, compared to wild type retinas. α-tubulin was used as loading control. (B) Ultrastructural analysis by means of transmission electron microscopy showed thinning and increased electron density of the capillary basement membrane of Sirt1-tg retinas. (C) Morphometric analysis confirmed basement membrane thinning in Sirt1-tg retinal capillaries (0.137 ± 0.10 μm VS 0.100 ± 0.10 μm; n = 3 animals per group, 5-7 capillaries per animal). (D) Confocal microscopy analysis of whole mount retinas immunohistochemically labelled with anti-collagen type IV antibody (green) showed focal deposition of collagen IV (arrowheads) in the basement membrane of retinal vessels from Sirt1-tg mice. Data presented as mean ± SEM. Asterisks indicate statistically significant differences: *p < 0.05. WT: wild type; BM: basement membrane; EC: endothelial cell. L: capillary lumen. Scale bars: B(WT) = 0.361 μm; B(Sirt1-tg) = 0.373 μm; D = 27.19 μm.

(Pfluger et al., 2008). Although Pfluger and colleagues reasoned that interference of the co-expressed Dnajc12 is of little relevance (Pfluger et al., 2008), it has been shown that certain naturally occurring isoforms of this gene have pro-survival effects by increasing resistance to ferroptosis and apoptosis induced by chemotherapy in breast cancer (Shen et al., 2024). Therefore, we cannot rule out the possibility of whether the pro-survival effect of Sirt1 observed in our study may have further increase by the chaperone protein activity of the overexpressed Dnajc12.

5. Conclusions

This study showed that Sirt1 overexpression is associated with increased VEGF expression in the retina of Sirt1-tg mice. However, this increase in VEGF does not appear to be accompanied by a detectable angiogenic response. In this context, our findings indicate that Sirt1 overexpression may be linked to features consistent with vessel stabilization, including increased pericyte coverage and enhanced collagen IV deposition in the vascular basement membrane. Together, these observations support a potential role for Sirt1 as a modulator of VEGF activity, possibly favouring its protective effects while limiting angiogenic responses through mechanisms related to vessel stabilization.

Funding

Supported by the Ministerio de Cultura e Innovación, Spain (grant number PID 2021-122545OB-100); Fundação para a Ciência e a Tecnologia (SFRH/BPD/102573/2014, SFRH/BD/95330/2013), Ministerio da Educação e Ciência, Portugal; and Fondo Europeo de Desarrollo Regional (FEDER).

CRediT authorship contribution statement

Joana Catita: Data curation, Formal analysis, Investigation, Writing – original draft. **Andreia Valença:** Formal analysis, Investigation. **Mariana López-Luppo:** Investigation. **Víctor Nacher:** Writing – review & editing. **Aina Bonet:** Investigation. **Ana Carretero:** Investigation, Writing – review & editing. **Patricia Jaramillo-Garcés:** Investigation. **Marc Navarro:** Writing – review & editing. **Fernando Faus:** Writing – review & editing. **Luísa Mendes-Jorge:** Writing – review & editing. **David Ramos:** Formal analysis, Investigation, Validation, Visualization, Writing – original draft, Writing – review & editing. **Jesús Ruberte:** Conceptualization, Funding acquisition, Project administration, Resources, Supervision, Validation, Visualization, Writing – original draft, Writing – review & editing.

Declaration of competing interest

The authors declare that they have no known competing financial interests or personal relationships that could have appeared to influence the work reported in this paper.

Acknowledgements

The authors thank Lorena Noya, Angel Vazquez, Veronica Melgarejo, Daniela Calderón, and Munachimso Kalu Njasi for technical assistance.

Appendix A. Supplementary data

Supplementary data to this article can be found online at https://doi.org/10.1016/j.exer.2026.111177.

Data availability

Data will be made available on request.

References

Adachi, E., Hopkinson, I., Hayashi, T., 1997. Basement-membrane stromal relationships: interactions between collagen fibrils and the Lamina densa. Int. Rev. Cytol. 173, 73–156.

Adamis, A.P., Miller, J.W., Bernal, M.-T., D'Amico, D.J., Folkman, J., Yeo, T.-K., Yeo, K. T., 1994. Increased vascular endothelial growth factor levels in the vitreous of eyes with proliferative diabetic retinopathy. Am. J. Ophthalmol. 118 (4), 445–450.

Adu-Agyeiwaah, Y., Vieira, C.P., Asare-bediako, B., Li Calzi, S., DuPont, M., Floyd, J., Boye, S., Chiodo, V., Busik, J.V., Grant, M.B., 2023. Intravitreal administration of AAV2-SIRT1 reverses diabetic retinopathy in a mouse model of type 2 diabetes. Transl. Vis. Sci. Technol. 12 (4), 20.

Aiello, L.P., Avery, R.L., Arrigg, P.G., Keyt, B.A., Jampel, H.D., Shah, S.T., Pasquale, L.R., King, G.L., 1994. Vascular endothelial growth factor in ocular fluid of patients with diabetic retinopathy and other retinal disorders. N. Engl. J. Med. 331 (22), 1480–1487.

Amadio, M., Govoni, S., Pascale, A., 2016. Targeting VEGF in eye neovascularization: what's new?: a comprehensive review on current therapies and oligonucleotide-based interventions under development. Pharmacol. Res. 103, 253–269.

Andrae, J., Gallini, R., Betsholtz, C., 2008. Role of platelet-derived growth factors in physiology and medicine. Genes Dev. 22 (10), 1276–1312.

Armulik, A., Abramsson, A., Betsholtz, C., 2005. Endothelial/Pericyte interactions. Circ. Res. 97 (6), 512–523.

Armulik, A., Genové, G., Betsholtz, C., 2011. Pericytes: developmental, physiological, and pathological perspectives, problems, and promises. Dev. Cell 21 (2), 193–215.

Bahramsoltani, M., Slosarek, I., De Spiegelaere, W., Plendl, J., 2014. Angiogenesis and collagen type IV expression in different endothelial cell culture systems. Anat. Histol. Embryol. 43 (2), 103–115.

Benjamin, L.E., Hemo, I., Keshet, E., 1998. A plasticity window for blood vessel remodeling is defined by pericyte coverage of the preformed endothelial network and is regulated by PDGF-B and VEGF. Development (Camb.) 125 (9), 1591–1598.

Betsholtz, C., 2004. Insight into the physiological functions of PDGF through genetic studies in mice. Cytokine Growth Factor Rev. 15 (4), 215–228.

Bonanno, E., Iurlaro, M., Madri, J.A., Nicosia, R.F., 2000. Type IV collagen modulates angiogenesis and neovessel survival in the rat aorta model. In Vitro Cell. Dev. Biol. Anim. 36 (5), 336–340.

Brooks, C.L., Gu, W., 2009. How does SSIRT1 affect metabolism, senescence, and cancer? Nat. Rev. Cancer 9 (2), 123–128.

Budd, S.J., Hartnett, M.E., 2010. Increased angiogenic factors during avascular retina prior to neovascularization in ROP model. Arch. Ophthalmol. 128 (5), 589–595.

Caporarello, N., D'Angeli, F., Cambria, M.T., Candido, S., Giallongo, C., Salmeri, M., Lombardo, C., Longo, A., Giurdanella, G., Anfuso, C.A., Lupo, G., 2019. Pericytes in microvessels: from "mural" function to brain and retina regeneration. Int. J. Mol. Sci. 20 (24), 6351. https://doi.org/10.3390/ijms20246351.

Chang, H.-C., Guarente, L., 2014. SIRT1 and other sirtuins in Metabolism. Trends Endocrinol. Metabol. 25 (3), 138–145.

Chekenya, M., Hjelstuen, M., Enger, P.Ø., Thorsen, F., Jacob, A.L., Probst, B., Haraldseth, O., Pilkington, G., Butt, A., Levine, J.M., Bjerkvig, R., 2002. NG2 proteoglycan promotes angiogenesis-dependent tumor growth in CNS by sequestering angiostatin. FASEB J. 16, 586–588.

Chen, J., Michan, S., Juan, A.M., Hurst, C.G., Hatton, C.J., Pei, D.T., Joyal, J.S., Evans, L. P., Cui, Z., Stahl, A., Sapieha, P., Sinclair, D.A., Smith, L.E., 2013. Neuronal sirtuin 1 mediates retinal vascular regeneration in oxygen-induced ischemic retinopathy. Angiogenesis 16 (4), 985–992.

Cui, C., Li, Y., Liu, Y., 2019. Down-regulation of miR-377 suppresses high glucose and hypoxia-induced angiogenesis and inflammation in human retinal endothelial cells by direct up-regulation of target gene SIRT1. Hum. Cell 33 (3), 260–274.

D'Onofrio, N., Vitiello, M., Casale, R., Servillo, L., Giovane, A., Balestrieri, M.L., 2015. Sirtuins in vascular diseases: emerging roles and therapeutic potential. Biochim. Biophys. Acta 1852 (7), 1311–1322.

Diaz-Flores, L., Gutierrez, R., Madrid, J.F., Varela, H., Valladares, F., Acosta, E., Martín-Vasallo, P., Díaz-Flores, Jr. L., 2009. Pericytes. Morphofunction, interactions and

pathology in a quiescent and activated mesenchymal cell niche. Histol. Histopathol. 24 (7), 909–969.
Domigan, C.K., Warren, C.M., Antanesian, V., Happel, K., Ziyad, S., Lee, S., Krall, A., Duan, L., Torres-Collado, A.X., Castellani, L.W., Elashoff, D., Christofk, H.R., van der Bliek, A.M., Potente, M., Iruela-Arispe, M.L., 2015. Autocrine VEGF maintains endothelial survival through regulation of metabolism and autophagy. J. Cell Sci. 128 (12), 2236–2248.
Dong, W., Li, N., Gao, D., Zhen, H., Zhang, X., Li, F., 2008. Resveratrol attenuates ischemic brain damage in the delayed phase after stroke and induces messenger RNA and protein express for angiogenic factors. J. Vasc. Surg. 48 (3), 709–714.
Dudley, A.C., Griffioen, A.W., 2023. The modes of angiogenesis: an updated perspective. Angiogenesis 26 (4), 477–480.
Enge, M., Bjarnegård, M., Gerhardt, H., Gustafsson, E., Kalén, M., Asker, N., Hammes, H. P., Shani, M., Fässler, R., Betsholtz, C., 2002. Endothelium-specific platelet-derived growth factor-B ablation mimics diabetic retinopathy. EMBO J. 21 (6), 4307–4316.
Filipek, S., Stenkamp, R.E., Teller, D.C., Palczewski, K., 2003. G protein-coupled receptor rhodopsin: a prospectus. Annu. Rev. Physiol. 65, 851–879.
Finkel, T., Deng, C.X., Mostoslavsky, R., 2009. Recent progress in the biology and physiology of sirtuins. Nature 460 (7255), 587–591.
Foxton, R.H., Finkelstein, A., Vijay, S., Dahlmann-Noor, A., Khaw, P.T., Morgan, J.E., Shima, D.T., Ng, Y.S., 2013. VEGF-A is necessary and sufficient for retinal neuroprotection in models of experimental glaucoma. Am. J. Pathol. 182 (4), 1379–1390.
Fukushi, J.I., Makagiansar, I.T., Stallcup, W.B., 2004. NG2 Proteoglycan promotes endothelial cell motility and angiogenesis via engagement of Galectin-3 and α3β1 integrin. Mol. Biol. Cell 15, 3580–3590.
Gaengel, K., Genové, G., Armulik, A., Betsholtz, C., 2009. Endothelial-mural cell signaling in vascular development and angiogenesis. Arterioscler. Thromb. Vasc. Biol. 29 (5), 630–638.
Geevarghese, A., Herman, I.M., 2014. Pericyte-Endothelial Cross-Talk: implications and opportunities for advanced cellular therapies. Transl. Res. 163 (4), 296–306.
Gerber, H.P., McMurtrey, A., Kowalski, J., Yan, M., Keyt, B.A., Dixit, V., Ferrara, N., 1998. Vascular endothelial growth factor regulates endothelial cell survival through the phosphatidylinositol 3*-Kinase/Akt signal transduction pathway. J. Biol. Chem. 273 (46), 30336–30343.
Gerhard, H., Betsholtz, C., 2003. Endothelial-pericyte interactions in angiogenesis. Cell Tissue Res. 314 (1), 15–23.
Grant, R.I., Hartman, D.A., Underly, R.G., Berthiaume, A.-A., Bhat, N.R., Shih, A.Y., 2019. Organizational hierarchy and structural diversity of microvascular pericytes in adult mouse cortex. J. Cereb. Blood Flow Metab. 39 (3), 411–425.
Hammes, H.P., Martin, S., Federlin, K., Geisen, K., Brownlee, M., 1991. Aminoguanidine treatment inhibits the development of experimental diabetic retinopathy. Proc. Natl. Acad. Sci. USA 88 (24), 11555–11558.
Hartmann, D.A., Coelho Santos, V., Shih, A.Y., 2022. Pericyte control of blood flow across microvascular zones in the central nervous system. Annu. Rev. Physiol. 84, 331–354.
Hellström, M., Kalén, M., Lindahl, P., Abramsson, A., Betsholtz, C., 1999. Role of PDGF-B and PDGFR-β in recruitment of vascular smooth muscle cells and pericytes during embryonic blood vessel formation in the mouse. Development (Camb.) 126, 3047–3055.
Hirschi, K.K., Rohovsky, S.A., D'Amore, P., 1997. Cekell interactions in vessel assembly: a model for the fundamentals of vascular remodelling. Transpl. Immunol. 5, 177–178.
Huang, F.-J., You, W.-K., Bonaldo, P., Seyfried, T.N., Pasquale, E.B., Stallcup, W.B., 2010. Pericyte deficiencies lead to aberrant tumor vascularization in the brain of the NG2 null mouse. Dev. Biol. 344 (2), 1035–1046.
Hughes, S., Chan-Ling, T., 2004. Characterization of smooth muscle cell and pericyte differentiation in the rat retina in vivo. Investig. Ophthalmol. Vis. Sci. 45 (8), 2795–2806.
Hwang, J., Lee, S.-Y., Choi, J.-R., Shin, K.S., Choi, C.Y., Kang, S.J., 2013. SIRT1 negatively regulates the protein stability of HIPK2. Biochem. Biophys. Res. Commun. 441 (4), 799–804.
Jain, R.K., 2003. Molecular regulation of vessel maturation. Nat. Med. 9 (6), 685–693.
Jaliffa, C., Amegrane, I., Dansault, A., Leemput, J., Vieira, V., Lacassagne, E., Provost, A., Bigot, K., Masson, C., Menasche, M., Abitbol, M., 2009. Investig. Ophthalmol. Vis. Sci. 50 (8), 3562–3572.
Keck, P.J., Hauser, S.D., Krivi, G., Sanzo, K., Warren, T., Feder, J., Connolly, D.T., 1989. Vascular permeability factor, an endothelial cell mitogen related to PDGF. Science 246, 1309–1312.
Kofler, N.M., Shawber, C.J., Kangsamaksin, T., Reed, H.O., Galatioto, J., Kitajewski, J., 2011. Notch signaling in developmental and tumor angiogenesis. Genes Cancer 2 (12), 1106–1116.
Kolluru, G.K., Bir, S.C., Kevil, C.G., 2012. Endothelial dysfunction and diabetes: effects on angiogenesis, vascular remodeling, and wound healing. Int. J. Vasc. Med. 2012, 918267.
Kowluru, R.A., Santos, J.M., Zhong, Q., 2014. Sirt1, a negative regulator of matrix metalloproteinase-9 in diabetic retinopathy. Investig. Ophthalmol. Vis. Sci. 55 (9), 5653–5660.
Kuwabara, T., Cogan, D.G., 1960. Studies of retinal vascular patterns part I. Normal architecture. Arch. Ophtalmol. 64 (6), 904–911.
Kvanta, A., Algvere, P.V., Berglin, L., Seregard, S., 1996. Subfoveal fibrovascular membranes in age-related macular degeneration express vascular endothelial growth factor. Investig. Ophthalmol. Vis. Sci. 37 (9), 1929–1934.
Law, M., Wang, P.-C., Zhou, Z.-Y., Wang, Y., 2024. From microcirculation to aging-related diseases: a focus in endothelial SIRT1. Pharmaceuticals 17, 1495.
Lee, C., Kim, M.-J., Kumar, A., Lee, H.-W., Yang, Y., Kim, Y., 2025. Vascular endothelial growth factor signaling in health and disease: from molecular mechanisms to therapeutic perspectives. Signal Transduct. Targeted Ther. 10, 170.
Lee, S., Chen, T.T., Barber, C.L., Jordan, M.C., Murdock, J., Desai, S., Ferrara, N., Nagy, A., Roos, K.P., Iruela-Arispe, M.L., 2007. Autocrine VEGF signaling is required for vascular homeostasis. Cell 130 (4), 691–703.
Leung, D.W., Cachianes, G., Kuang, W.J., Goeddel, D.V., Ferrara, N., 1989. Vascular endothelial growth factor is a secreted angiogenic mitogen. Science 246, 1306–1309.
Li, G., Gao, J., Ding, P., Gao, Y., 2025. The role of endothelial cell-pericyte interactions in vascularization and diseases. J. Adv. Res. 67, 269–288.
Li, Y., Wang, K., Feng, Y., Fan, C., Wang, F., Yan, J., Yang, J., Pei, H., Liang, Z., Jiang, S., Cheng, X., Yang, Y., Qua, Y., 2014. Novel role of silent information regulator 1 in acute endothelial cell oxidative stress injury. Biochim. Biophys. Acta 1842, 2246–2256.
Lim, J.-H., Lee, Y.-M., Chun, Y.-S., Chen, J., Kim, J.-E., Park, J.-W., 2010. Sirtuin 1 modulates cellular responses to hypoxia by deacetylating hypoxia-inducible factor 1α. Mol. Cell 38, 864–878.
Lindahl, P., Johansson, B.R., Levéen, P., Betsholtz, C., 1997. Pericyte loss and microaneurysm formation in PDGF-B-deficient mice. Science 277 (5323), 242–245.
Mai-Morente, S.P., Marset, V.M., Blanco, F., Isasi, E.E., Abudara, V., 2021. A nuclear fluorescent dye identifies pericytes at the neurovascular unit. J. Neurochem. 157 (4), 1377–1391.
Maloney, S.C., Antecka, E., Odashiro, A.N., Fernandes, B.F., Doyle, M., Lim, L.A., Katib, Y., Burnier Jr., M.N., 2012. Expression of SIRT1 and DBC1 in developing and adult retinas. Stem Cell. Int. 2012, 908183.
McLenachan, S., Magno, A.L., Ramos, D., Catita, J., McMenamin, P.G., Chen, F.K., Rakoczy, E.P., Ruberte, J., 2015. Angiography reveals novel features of the retinal vasculature in healthy and diabetic mice. Exp. Eye Res. 138, 6–21.
Mercier, C., Brazeau, T., Lamoureux, J., Boisvert, E., Robillard, S., Breton, V., Paré, M., Guay, A., Lizotte, F., Despatis, M.-A., Geraldes, P., 2021. Diabetes impaired ischemia-induced PDGF (Platelet-Derived growth factor) signaling actions and vessel formation through the activation of Scr homology 2-Containing Phosphatase-1. Arterioscler. Thromb. Vasc. Biol. 41, 2469–2482.
Michan, S., Sinclair, D., 2007. Sirtuins in mammals: insights into their biological function. Biochem. J. 404 (1), 1–13.
Michishita, E., Park, J.Y., Burneskis, J.M., Barrett, J.C., Horikawa, I., 2005. Evolutionarily conserved and nonconserved cellular localizations and functions of human SIRT proteins. Mol. Biol. Cell 16 (10), 4623–4635.
Miller, J.W., Adamis, A.P., Shima, D.T., D'Amore, P.A., Moulton, R.S., O'Reilly, M.S., Folkman, J., Dvorak, H.F., Brown, L.F., Berse, B., Yeo, T.-K., Yeo, K.-T., 1994. Vascular endothelial growth factor/vascular permeability factor is temporally and spatially correlated with ocular angiogenesis in a primate model. Am. J. Pathol. 145 (3), 574–584.
Mishra, M., Duraisamy, A.J., Kowluru, R.A., 2018. Sirt1: a guardian of the development of diabetic retinopathy. Diabetes 67 (4), 745–754.
Mizutani, M., Gerhardinger, C., Lorenzi, M., 1998. Müller cell changes in human diabetic retinopathy. Diabetes 47 (3), 445–449.
Morona, R., Moreno, N., Lopez, J.M., Muñoz, M., Domínguez, L., González, A., 2008. Calbindin-D28k and calretinin as markers of retinal neurons in the anuran amphibian Rana perezi. Brain Res. Bull. 75 (2–4), 379–383.
Nadal-Nicolás, F.M., Jimenez-Lopez, M., Sobrado-Calvo, P., Nieto-Lopez, L., Cánovas-Martinez, I., Salinas-Navarro, M., Vidal-Sanz, M., Agudo, M., 2009. Brn3a as a marker of retinal ganglion cells: qualitative and quantitative time course studies in naive and optic nerve-injured retinas. Investig. Ophthalmol. Vis. Sci. 50 (8), 3860–3868.
Oellerich, M.F., Potente, M., 2012. FOXOs and sirtuins in vascular growth, maintenance and aging. Circ. Res. 110 (9), 1238–1251.
Ohsawa, K., Imai, Y., Nakajima, K., Kohsaka, S., 1997. Generation and characterization of a microglial cell line, MG5, derived from a p53-deficient mouse. Glia 21 (3), 285–298.
Ohtoshi, A., Wang, S.W., Maeda, H., Saszik, S.M., Frishman, I.J., Klein, W.H., Behringer, R.R., 2004. Regulation of retinal cone bipolar cell differentiation and photopic vision by the CVC homeobox gene VSx1. Curr. Biol. 14 (6), 530–536.
Orimo, M., Minamino, T., Miyauchi, H., Tateno, K., Okada, S., Moriya, J., Komuro, I., 2009. Protective role of SIRT1 in diabetic vascular dysfunction. Arterioscler. Thromb. Vasc. Biol. 29 (6), 889–894.
Ozerdem, U., Grako, K.A., Dahlin-Huppe, K., Monosov, E., Stallcup, W.B., 2001. NG2 proteoglycan is expressed exclusively by mural cells during vascular morphogenesis. Dev. Dyn. 222 (2), 218–227.
Pan, Q., Gao, Z., Zhu, C., Peng, Z., Song, M., Li, L., 2020. Overexpression of histone deacetylase SIRT1 exerts an antiangiogenic role in diabetic retinopathy via miR-20a elevation and YAP/HIF1α/VEGFA depletion. Am. J. Physiol. Endocrinol. Metab. 319 (5), E932–E943.
Pfister, F., Feng, Y., vom Hagen, F., Hoffmann, S., Molema, G., Hillebrands, J.-L., Shani, M., Deutsch, U., Hammes, H.P., 2008. Pericyte migration: a novel mechanism of pericyte loss in experimental diabetic retinopathy. Diabetes 57, 2495–2502.
Pfluger, P.T., Herranz, D., Velasco-Miguel, S., Serrano, M., Tschöp, M.H., 2008. Sirt1 protects against high-fat diet-induced metabolic damage. Proc. Natl. Acad. Sci. USA 105 (28), 9793–9798.
Potente, M., Ghaeni, L., Baldessari, D., Mostoslavsky, R., Rossig, L., Dequiedt, F., Haendeler, J., Mione, M., Dejana, E., Alt, F.W., Zeiher, A.M., Dimmeler, S., 2007. SIRT1 controls endothelial angiogenic functions during vascular growth. Genes Dev. 21 (20), 2644–2658.
Purves, D., Augustine, G.J., Fitzpatrick, D., Hall, W.C., LaMantia, A.S., McNamara, J.O., Williams, S.M., 2004. Neuroscience; Vision – the Eye, third ed. Sinauer Associates, Sunderland, MA, pp. 229–258.

Pusztaszeri, M.P., Seelentag, W., Bosman, F.T., 2006. Immunohistochemical expression of endothelial markers CD31, CD34, von Willebrand factor, and Fli-1 in normal human tissues. J. Histochem. Cytochem. 54 (4), 385–395.
Rakic, J.-M., Lambert, V., Devy, L., Luttun, A., Carmeliet, P., Claes, C., Nguyen, L., Foidart, J.-M., Noël, A., Munaut, C., 2003. Placental growth factor, a member of the VEGF family, contributes to the development of choroidal neovascularization. Investig. Ophthalmol. Vis. Sci. 44 (7), 3186–3193.
Ribatti, D., Nico, B., Crivellato, E., 2011. The role of pericytes in angiogenesis. Int. J. Dev. Biol. 55, 261–268.
Sarthy, P.V., Fu, M., Huang, J., 1991. Developmental expression of glial fibrillary acidic protein (GFAP) gene in the mouse retina. Cell. Mol. Neurobiol. 11 (6), 623–637.
Shen, M., Cao, S., Long, X., Xiao, L., Yang, L., Zhang, P., Li, L., Chen, F., Lei, T., Gao, H., Ye, F., Bu, H., 2024. DNAJC12 causes breast cancer chemotherapy resistance by repressing doxorubicin-induced ferroptosis and apoptosis via activation of AKT. Redox Biol. 70, 103035.
Shepro, D., Morel, M.M., 1993. Pericyte physiology. FASEB J. 7 (11), 1031–1038.
Shibuya, M., 2008. Vascular endothelial growth factor-dependent and -independent regulation of angiogenesis. BMB Rep. 41 (4), 278–286.
Siperstein, M.D., Unger, R.H., Madison, L.L., 1968. Studies of muscle capillary basement membranes in normal subjects, diabetic, and prediabetic patients. J. Clin. Investig. 47, 1973–1999.
Skalli, O., Pelte, M.F., Peclet, M.C., Gabbiani, G., Gugliotta, P., Bussolati, G., Ravazzola, M., Orci, L., 1989. Alpha-smooth muscle actin, a differentiation marker of smooth muscle cells, is present in microfilamentous bundles of pericytes. J. Histochem. Cytochem. 37 (3), 315–321.
Stallcup, W.B., 2018. The NG2 proteoglycan in pericyte biology. In: Birbrair, A. (Ed.), Pericyte Biology - Novel Concepts, Advances in Experimental Medicine and Biology, 1109. Springer, Cham, pp. 5–19.
Stapor, P.C., Sweat, R.S., Dashti, D.C., Betancourt, A.M., 2014. Pericyte dynamics during angiogenesis. J. Vasc. Res. 51, 163–174.
Stein, S., Schäfer, N., Breitenstein, A., Besler, C., Winnik, S., Lohmann, C., Heinrich, K., Brokopp, C.E., Handschin, C., Landmesser, U., Tanner, F.C., Lüscher, T.F., Matter, C. M., 2010. SIRT1 reduces endothelial activation without affecting vascular function in ApoE-/- mice. Aging 2 (6), 353–360.
Tălu, S., Vlăduţiu, C., Lupaşcu, C.A., 2015. Characterization of human retinal vessel arborisation in normal and amblyopic eyes using multifractal analysis. Int. J. Ophthalmol. 8 (5), 996–1002.
Tanii, M., Yonemitsu, Y., Fujii, T., Shikada, Y., Kohno, R., Onimaru, M., Okano, S., Inoue, M., Hasegawa, M., Onohara, T., Maehara, Y., Sueishi, K., 2006. Diabetic microangiopathy in ischemic limb is a disease of disturbance of the platelet-derived growth Factor-BB/Protein kinase C axis but not of impaired expression of angiogenic factors. Circ. Res. 98, 55–62.
von Tell, D., Armulik, A., Betsholtz, C., 2006. Pericytes and vascular stability. Exp. Cell Res. 312 (5), 623–629.
Wang, P., Du, H., Zhou, C.-C., Song, J., Liu, X., Cao, X., Mehta, J.L., Shi, Y., Su, D.-F., Miao, C.-Y., 2014. Intracellular NAMPT-NAD+-SIRT1 cascade improves post-ischaemic vascular repair by modulating Notch signaling in endothelial progenitors. Cardiovasc. Res. 104 (3), 477–488.
Wang, P., Li, C., Deng, Y., Yu, Q., Meng, X., Jiang, T., Wang, Q., Fu, Y., 2022. Effect of plasma-derived extracellular vesicles of angiogenesis and the ensuing proliferative diabetic retinopathy through a miR-30b-dependent mechanism. Diabetol. Metab. Syndr. 14 (1), 188.
You, W.-K., Yotsumoto, F., Sakimura, K., Adams, R.H., Stallcup, W.B., 2014. NG2 proteoglycan promotes tumor vascularization via integrin-dependent effects on pericyte function. Angiogenesis 17, 61–76.
Zhang, T., Kraus, W.L., 2010. SIRT1-dependent regulation of chromatin and transcription: linking NAD+ metabolism and signaling to the control of cellular functions. Biochim. Biophys. Acta 1804 (8), 1666–1675.
Zhu, S., Chen, M., Ying, Y., Wu, Q., Huang, Z., Ni, W., Wang, X., Xu, H., Bennett, S., Xiao, J., Xu, J., 2022. Versatile subtypes of pericytes and their roles in spinal cord injury repair, bone development and repair. Bone Res. 10, 30.
Zimmerman, K.W., 1923. Der feinere Bau der Blutcapillaren. Z. Anat. Entwicklungsgeschichte 68 (1), 29–109.
Zudaire, E., Gambardella, L., Kurcz, C., Vermeren, S., 2011. A computational tool for quantitative analysis of vascular networks. PLoS One 6 (11), e27385.